The Eldgjá lava flow beneath Mýrdalssandur, S-Iceland

- Mapping with magnetic measurements -

Sigrún Sif Sigurðardóttir

Faculty of Earth Sciences
University of Iceland
2014

The Eldgjá lava flow beneath Mýrdalssandur, S-Iceland

- Mapping with magnetic measurements -

Sigrún Sif Sigurðardóttir

60 ECTS thesis submitted in partial fulfillment of a *Magister Scientiarum* degree in Geology

Advisors
Magnús Tumi Guðmundsson
Sigrún Hreinsdóttir

Faculty of Earth Sciences
School of Engineering and Natural Sciences
University of Iceland
Reykjavík, October 2014

The Eldgjá lava flow beneath Mýrdalssandur, S-Iceland
- Mapping with magnetic measurements -
60 ECTS thesis submitted in partial fulfillment of a *Magister Scientiarum* degree in Geology

Faculty of Earth Sciences
School of Engineering and Natural Sciences
University of Iceland
Sturlugata 7
101, Reykjavík
Iceland

Telephone: 525 4700

Bibliographic information:
Sigrún Sif Sigurðardóttir, 2014, *The Eldgjá lava flow beneath Mýrdalssandur, S-Iceland, - Mapping with magnetic measurements* -, Master's thesis, Faculty of Earth Sciences, University of Iceland, pp. 52.

Printing: Háskólaprent
Reykjavík, Iceland, October 2014

Declaration

Hereby I declare that this thesis is written by me and that it has neither by part nor the whole been submitted previously to a higher degree.

Sigrún Sif Sigurðardótti

Abstract

In this study the buried edge of the Álftaver lava flow below Mýrdalssandur is located with magnetic measurements. The Álftaver lava flow was produced in the Eldgjá eruption 934 AD, which is one of the largest flood lava eruptions in the last 1100 years. The lava flow was formed in several eruptive events during a 3-8 year period. Most recent volume estimates put it at ~18 km^3. The lava followed rivers and gorges down to the lowlands of Álftaver, Landbrot and Meðalland and formed large lava fields called the Eldgjá lava flow. The lava fields raised the topography, dammed rivers and altered their flow pattern. Since the eruption sediments have accumulated at Mýrdalssandur from jökulhlaups coming from beneath the Kötlujökull glacier. At first the Álftaver lava was a barrier for jökulhlaups from flowing across it to the east. However, Mýrdalssandur built up quickly until the floods were able to flow over the Álftaver lava flow. Thus, a part of the lava flow is now buried beneath Mýrdalssandur.

In total 14 magnetic profiles were measured with a proton magnetometer and GPS. The total length of the profiles measured is ~75 km. The measurements were conducted across previously determined, 1-15 km long profiles, lying approximately perpendicular to the edge of the lava flow. The measurements were for the most part performed on foot and partly by car. Measurements were done at 2 sec intervals where the total magnetic field in nT and the GPS position was measured. The principle aim of the survey was identifying changes in depth to magnetic sources. Segments of individual profiles with similar spacing of anomalies (spatial frequency) and anomaly amplitudes were identified visually on the profiles. Changes in spatial frequency were used to identify the location of the buried lava edge as well as lava ledges. Maximum depth to magnetic sources was estimated with the Peters half slope method.

The measurements revealed the edge further to the west than previously assumed. The lava edge was found ~5 km east of Hafursey and ~8 km south of Rjúpnafell. Depth estimations reveal that the top of the lava edge lies at 10 m depth. The depth to the lava flow generally decreases towards the east and northeast with several exceptions. A couple of profiles show evidence of the Kriki hyaloclastite flow beneath the sand plain. The depth to the lava flow suggests that sediment accumulation on central and western Mýrdalssandur has been 4 – 5 km^3 since the Eldgjá lava flow was emplaced. According to the magnetic measurements the area of the buried lava flow is 64 km^2 and the volume of this buried lava is 1.4 +/- 0.3 km^3. If this buried lava is added to previous estimates the area increases to 844 km^2 and the volume becomes 19.7 km^3. This underlines the size and the great importance of the Eldgjá eruption in Iceland's geological history.

Útdráttur

Í þessari rannsókn er jaðar Álftaver hrauns undir Mýrdalssandi fundinn og staðsettur með segulmælingum. Álftaver hraunið myndaðist í Eldgjárgosinu sem talið er hafa hafist árið 934 og er eitt af stærstu flæðigosum sem þekkt eru á síðustu 1100 ár. Hraunið myndaðist í nokkrum goshrinum á 3-8 ára tímabili. Hraunið hefur verið metið um og yfir 18 km^3. Hraunið flæddi um árdali og gljúfur niður á láglendið í Álftaveri, Landbroti og Meðallandi og myndaði þar stórar hraunbreiður sem kallast Eldgjá hraun. Hraunbreiðurnar hækkuðu landslagið, stífluðu ár og breyttu flæðamynstri þeirra. Mikið set úr jökulhlaupum undan Kötlujökli hefur sest til á Mýrdalssandi síðan Eldgjárhraunið rann. Eftir gosið myndaði Álftavers hraunið fyrirstöðu fyrir hlaupin en Mýrdalssandur byggðist fljótt upp og hlaupin fóru að flæða yfir hraunið og kaffæra hluta þess í sandi. Hraunjaðar Eldgjárhrauns hefur því verið á reiki á jarðfræðikortum í gegnum tíðina. Vesturbrún hraunsins á köflum verður einungis fundin með jarðeðlisfræðilegri könnun.

Fjórtán segulsnið voru mæld á Mýrdalssandi með sjálfvirkum róteinda segulmæli og GPS. Heildarlengd sniðanna er ~75 km. Mælt var í fyrirfram ákveðnum, 1-15 km löngum sniðum, sem liggja því næst hornrétt á hraunjaðarinn. Mælingarnar fóru mest megnis fram gangandi en að hluta til á bíl. Mælingar voru teknar á 2 sek fresti þar sem heildar segulsvið í nT var mælt og staðsetning ákvörðuð með GPS. Megin áhersla rannsóknarinnar var að greina breytingar á dýpi niður á segulmagnað berg. Við greiningu gagnanna var sniðunum sjónrænt skipt í hluta þar sem hver hluti einkenndist af svipaðri sveifluvídd. Breytingar í sveifluvídd voru talin merki um hraunjaðar eða stall í hrauninu. Hámarksdýpt var síðan metin með reglu Peters.

Segulmælingarnar sýndu að vesturbrún Eldgjárhrauns liggur mun vestar en fyrr hefur verið talið. Hraunjaðar Álftaver hrauns kemur fram ~5 km austur af Hafursey og ~8 km suður af Rjúpnafelli. Dýptarákvarðanir á segulsniðunum sýna að efri hluti hraunjaðarins liggur á um 10 m dýpi. Dýpi niður á hraunið minnkar til austurs eða í átt að hinum sýnilega hraunjaðri með nokkrum undantekningum. Tvö snið gáfu vísbendingar um Krika hraunið undir sandinum. Upphleðsla sets á mið- og vestur hluta Mýrdalsands er metin sem 4 – 5 km^3 síðan Eldgjárhraunið rann. Samkvæmt segulmælingunum er flatarmál hraunsins undir Mýrdalssandi 64 km^2 og rúmmálið 1.4 +/- 0.3 km^3. Séu þessar tölur lagðar við fyrra mat, fæst að heildarflatarmálið er 844 km^2 og rúmmálið 19.7 km^3 sem undirstrikar enn frekar stærð og mikilvægi eldgossins í jarðsögu Íslands.

Aknowledgements

Firstly I would like to thank my advisors Magnús Tumi Guðmundsson and Sigrún Hreinsdóttir for their help, guidance and financial support for the study. I would like to thank Páll Einarsson because he came up with the idea for this study. I want to thank all the people who assisted me during and in the preparation of the fieldwork on Mýrdalssandur. They were Hildur María Friðriksdóttir, Þorbjörg Ágústsdóttir, Vignir Val Steinarsson and last but not least Sveinbjörn Steinþórsson and Þorsteinn Jónsson. I would also like to thank Guðrún Larsen for her help and contribution to the study. Additionally thanking Ómar Bjarki Smárason for showing me around the borehole sites at Mýrdalssandur east of Dýralækir. Lastly, I would like to thank Þorgils Jónasson at the National Energy Authority for access to borehole data.

Table of Contents

List of Figures

List of Tables

1 Introduction

Volcanic activity in south and southeast Iceland outside central volcanoes is dominated by fissure eruptions, often phreatomagmatic in character, occurring both subglacially and subaerially. Most of the activity occurs in the Eastern Volcanic Zone (EVZ). It has the highest volcanic activity and productivity of the volcanic zones in Iceland (Thordarson and Höskuldsson, 2008), thus, rapid buildup characterizes its stratigraphy. The area includes two of the largest glaciers in Iceland, the Vatnajökull and Mýrdalsjökull glaciers. The stratigraphy includes hyaloclastite, lava flows and sediments carried by jökulhlaups and river discharge. Many eruptions occur subglacially producing melt water, which escapes in jökulhlaups to the oceans. Continued jökulhlaups during Postglacial time have produced the sand plains in the southern lowlands (Jakobsson, 1979).

One of the largest flood lava eruptions in the last millennium is the Eldgjá eruption that occurred in the Katla volcanic system in 934 AD and lasted for up to 8 years (Thordarson et al., 2001; Larsen, 2000; 2010). It produced the Eldgjá lava flow combined of the Álftaver-, Meðalland-, and Landbrot lava flows. Volume estimates has put the lava flow around 18 km^3 (Thordarson et al., 2001). The western edge of the Álftaver lava flow lies beneath Mýrdalssandur sand plain as it has been buried by repeated jökulhlaups from beneath Kötlujökull glacier due to continued volcanic activity at Katla (Larsen, 2000; 2010). Therefore, it is difficult to estimate the extent of the lava flow without drilling or geophysical prospecting. As a result its westerly extension and volume is not well determined. Magnetic measurements can be used for locating objects and geological features that are not visible on the surface, such as dykes and buried lava flows because of the high sensitivity of the anomaly shape to the depth to the magnetic sources (Hinze, et al. 2013). The aim of this study is to map the western margin of the 934 AD Eldgjá lava flow beneath the Mýrdalssandur sand plain in S-Iceland with magnetic measurements. In particular the study addresses the following:

1. The location of the western edge of the Eldgjá lava flow beneath Mýrdalssandur.
2. Provide better constraints on the size of the lava flow based on the location of the buried lava edge according to the magnetic measurements.
3. Provide an estimate of the rate of sediment accumulation on the central part of the Mýrdalssandur sand plain.
4. Evaluate the implications that the results have on the regional geology of the study area.

1.1 The geology of Iceland

Iceland is a volcanic island located in the North Atlantic Ocean. It is situated on top of a mantle plume and the mid-Atlantic ridge, a divergent plate boundary between the N-American plate and the Eurasian plate (Fig. 1.1) (Guðmundsson, 2000).

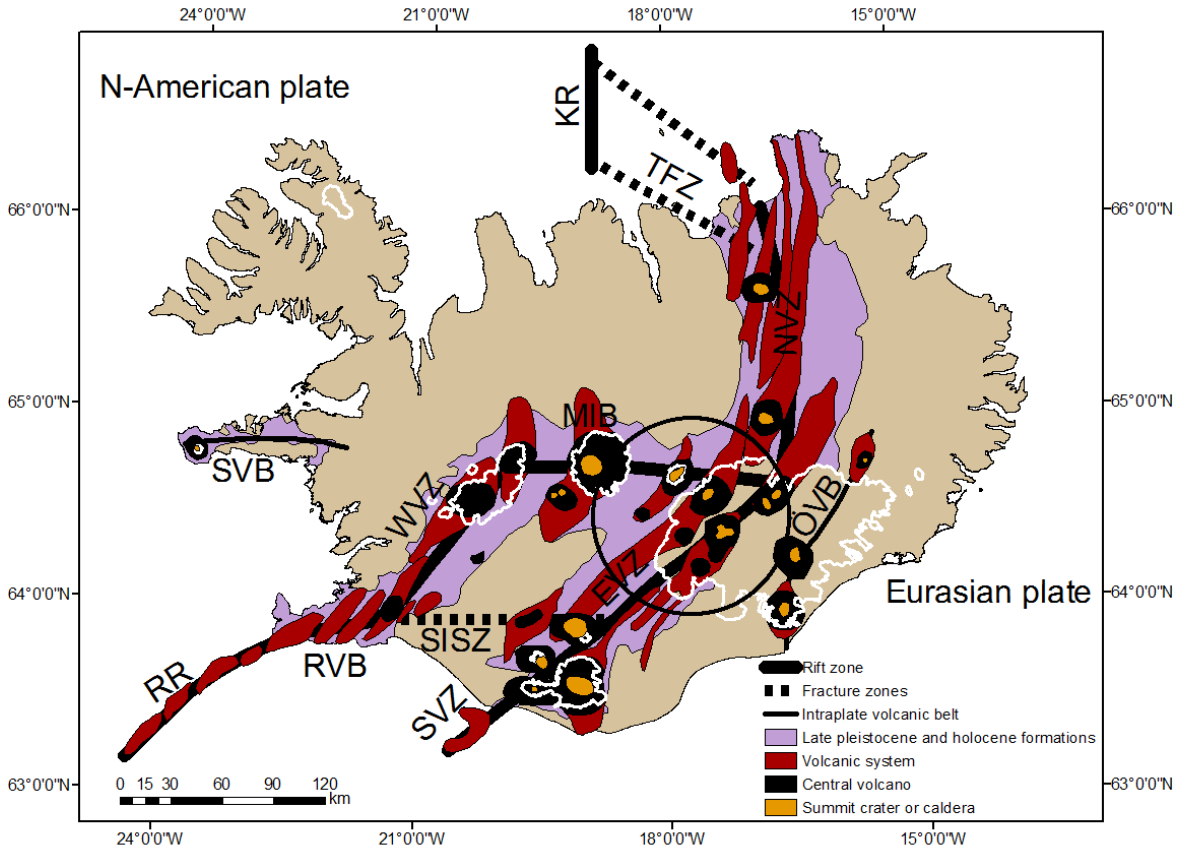

Figure 1.1: The geological setting of Iceland. The distribution of volcanic systems, central volcanoes, summit craters and calderas are s. Abbreviations: RR: Reykjanes Ridge, RVB: Reykjanes Volcanic Belt, SISZ: South Iceland Seismic Zone, WVZ: West Volcanic Zone, MIB: Mid-Iceland Belt, EVZ: East Volcanic Zone, SVZ: South Volcanic Zone, NVZ: North Volcanic Zone, TFZ: Tjörnes Fracture Zone, KR: Kolbeinsey Ridge, ÖVB: Öræfi Volcanic Belt and SVB: Snæfellsnes Volcanic Belt. The black open circle is the approximated location of the mantle plume. Based on Jóhannesson and Sæmundsson (1998); Sigmundsson (2006); Thordarson and Höskuldsson (2008).

The volcanic activity observed in Iceland is generated by the interaction between the ridge and the mantle plume, which is thought to extend to at least 400 km depth and possibly to the core-mantle boundary (Bjarnason, 2008). The relative motion of the ridge in respect to the hot spot leads to ridge jumps and propagating rifts (Einarsson, 1991). It is also responsible for the widening of the deformation zone where earthquakes and eruptions take place. However, the volcanic activity is focused along the ridge and at the center of the mantle plume (Einarsson, 2008; Jakobsdóttir, 2008). Volcanic activity in Iceland is confined to the neovolcanic zones, which are 15-50 km wide zones of active faulting and volcanism. The zones can be divided into three main segments, the Western Volcanic Zone (WVZ), the Northern Volcanic Zone (NVZ) and the Eastern Volcanic Zone (EVZ) (Guðmundsson, 2000; Thordarson and Larsen, 2007; Einarsson, 2008; Jakobsdóttir, 2008). The Reykjanes Volcanic belt (RVB) and the Mid-Iceland Belt (MIB) are less active zones. There are also three active intraplate volcanic belts, the Öræfi Volcanic Belt (ÖVB), Snæfellsnes Volcanic Belt (SVB) and the South Icelandic Volcanic Zone (Thordarson and Larsen, 2007; Einarsson, 2008; Thordarson and Höskuldsson, 2008). Most of the earthquakes that occur in Iceland take place along the seismic zones, the Tjörnes Fracture

Zone (TFZ), the South Iceland Seismic Zone, the Hengill Triple Junction and on the Reykjanes Peninsula. Other earthquakes are mostly related to volcanic activity at Iceland's volcanoes (Fig. 1.1) (Jakobsdóttir, 2008).

The volcanic activity takes place within the active volcanic zones, which are divided into several volcanic systems. The volcanic systems include a central volcano, where most of the activity takes place, and a fissure swarm (Einarsson, 1991; Guðmundsson, 2000). In the volcanic zones 30 active volcanic systems have been identified. The most active systems are Grímsvötn, Bárðabunga-Veiðivötn, Hekla and Katla based on both eruption frequency and volcanic productivity. These systems are all located in the EVZ. During the Holocene the EVZ has been by far the most active volcanic zone in Iceland (Thordarson and Larsen, 2007; Thordarson and Höskuldsson, 2008). The volcanic activity of the EVZ has been increasing during the last 3 million years while decreasing in the WVZ. This is a result of the relative movement of the mantle plume and the mid Atlantic ridge. The ridge tries to keep up with the movement of the mantle plume, which results in the formation of a new rift that with time takes over the activity of older zones. This cycle has occurred several times in Iceland's geological history. It has been suggested that the ÖVB is a new volcanic zone in formation (Einarsson, 1991; 2008).

The volcanism in Iceland is diverse but 75% of the eruptions that occur are subglacial explosive mafic eruptions (Thordarson and Larsen, 2007). The eruptions are typically small with limited effects on the environment and the climate. However, large eruptions do occur and they tend to take place on the fissure swarms outside the central volcano (Guðmundsson et al., 2008). Eruptions such as Laki (1783-1784) and Eldgjá (934 AD) fall into this category. They are the largest eruptions to take place in Iceland in historic times or in the last 11 centuries (Thordarson and Larsen, 2007).

2 The Katla volcanic system

The Katla volcanic system is located in the southern part of the EVZ and has been active for several hundred thousand years (Jakobsson, 1979). It comprises an ice covered central volcano and a 75 km long fissure swarm trending to the northeast (Larsen, 2000). The central volcano is thought to encompass a shallow magma chamber revealed by seismic undershooting (Guðmundsson et al., 1994) and magnetic measurements (Jónsson and Kristjánsson, 2000). It has a 110 km^2 and about 700 m deep caldera covered by the Mýrdalsjökull ice cap (Björnsson et al., 2000). It is not know exactly when the caldera formed but it was most likely during the last ice age or the Pleistocene. The formation is furthermore connected to the occurrence of a large eruption like the Eldgjá eruption (Sæmundsson, 1982). Seismic activity at Katla in recent years has been mostly confined to two locations, within the caldera and at Goðabunga at the western flank of the caldera (Jakobsdóttir, 2008). Katla is one of the most active volcanic systems (Thorarinson, 1975; Larsen, 2000, 2010; Óladóttir et al., 2005) with 21 confirmed eruptions since the settlement of Iceland (Table 2.1) (Thorarinsson, 1975; Larsen, 2000) and an average repose time of about 50 years (Elíasson et al., 2006). One eruption in the last 11 centuries was an effusive basaltic eruption. The other 20 were explosive phreatomagmatic basaltic eruptions (Larsen, 2000). Most of the explosive basaltic eruptions are small to moderate in size producing 0.01-1 km^3 of tephra (Thorarinsson, 1975; Larsen, 2010). However, a number of tephra layers originating from Katla have been found in the Greenland GRIP ice core, among others the large tephra layer known around the North Atlantic as the Vedde ash and in Iceland as the Skógar tephra (Norðdahl and Hafliðason, 1992; Grönvold et al., 1995; Hafliðason et al., 2000; Wastegård et al., 2000, 2002). Other Katla tephra layers have also been identified outside Iceland, e.g., the K1625, K1660 and K1755 eruptions (Thorarinsson, 1980, 1981; Hafliðasson et al., 2000). The last confirmed eruption at Katla took place in 1918 producing a 14 km high eruptive column. Jökulhlaups that occurred in 1955, 1999 and 2011 from Mýrdalsjökull glacier were possibly related to small subglacial eruptions but may also have been caused by changes in geothermal activity (Larsen, 2000; Guðmundsson and Larsen, 2013). Further discussion on the jökulhlaup activity from Katla is in Chapter 4.1.1.

Tephra layers from Katla are most often coal-black to brownish black in color, highly fragmented with limited amount of crystals (Larsen, 2000). Throughout Katla's volcanic history the eruptive material has been characterized by Fe-Ti transitional alkali basalts with a limited compositional range and mildly alkalic rhyolites (Jakobsson, 1979; Lacasse et al., 2006). Katla is, along with Öræfajökull and Askja, a clear example of a mixed magma suite with bimodal volcanism, making it easy to identify their deposit as tephra layers in soil sections on the basis of their chemical signature (Óladóttir et al., 2005; Lacasse et al., 2006).

Table 2.1: Confirmed historical eruptions in the Katla volcanic system (Larsen, 2000):

Year/century	Date	Length (days)	Preceeding years
K1918	October 12th	24	58
K1860	May 8th	20	37
K1823	June 26th	28	68
K1755	October 17th	~120	34
K1721	May 11th	>100	61
K1660	November 3rd	>60	35
K1625	September 2nd	13	13
K1612	October 12th		32
K1580	August 11th		80
K ~1500			
K 15th century			
K ~1440			(24)
K1416			(59)
K ~1357			(95)
K1262			17
K1245			(66)
K ~1179			
K 12th century			
E 934/938			
K ~920			(16)
K 9th century			

Tephrochronology has been used to construct Katla's Holocene explosive volcanic history (Larsen, 2000). More than 300 tephra layers have been found in the area around Katla. According to them the prehistoric explosive eruption frequency was higher than during historical time (Óladóttir et al., 2005). The system hasn't been stable during its history and has changed both in chemical composition and geometry. Eight evolutionary periods have been observed during the Holocene inferring three types of plumbing systems (Óladóttir et al., 2008). Each cycle begins at a stage with a simple plumbing system, which evolves to the second stage of a sill and dyke complex and eventually the system develops a magma chamber. The eruption frequency is highest during a sill and dyke complex but is lower during the other two stages. According to chemical analysis the Katla volcanic system now has a simple plumbing system (Óladóttir et al., 2008), contradicting seismic and magnetic measurements suggesting a shallow magma chamber (Guðmundsson et al., 1994; Jónsson and Kristjánsson, 2000). These changes between stages occur rapidly without any adjustment period and are possible connected to large eruptions in the system. The eight abrupt changes can be linked to the eight known Holocene lavas around Katla and among them are the Hólmsá (7700 years old) and Eldgjá (934 AD) lava flows (Jóhannesson and Sæmundsson, 1990; Óladóttir et al., 2008).

Katla has three main types of volcanic activity (Larsen, 2000). The most common events in the Katla volcanic system are the explosive phreatomagmatic basaltic eruptions. They occur on short fissures beneath Mýrdalsjökull inside the caldera. Accompanying the

eruptions are tephra fall and large jökulhlaups. The eruptions are characteristic eruption activity in the Holocene and more than 170 events have occurred (Larsen, 2000; 2010). The second most common events are explosive silicic eruptions. They occur on vents below the glacier and are fairly small with limited explosive activity. They produce thin tephra layers of fine ash, which were known as key marker layers in the regional tephrochronology before they were recognized as being produced by Katla. During the Holocene 12 silicic eruptions have occurred, however, no silicic eruptions have occurred since the Eldgjá eruption (Larsen, 2000; et al., 2001). The third and least common events in the system are effusive basaltic eruptions. They occur on the fissure swarm outside and at the margin of the caldera. They have an explosive period where tephra is produced and a period of lava outpouring (Miller, 1989; Larsen, 2000). Some 5 – 10 lava flows around Mýrdalssandur have been connected to eruptions at the Katla volcanic system. Most of the lava flows are small, a few km^2 to tens of km^2. The exceptions are large eruptions called fires that have produced large lava fields such as the Hólmsá and Eldgjá lava flows and the Kriki hyaloclastite flow. In total all lava flows from the Katla volcanic system cover an area of 890 km^2 (Jóhannesson and Sæmundsson, 1990; Óladóttir et al., 2008; Larsen, 2000; 2010). The Hólmsá lava field was produced in a fissure eruption, which is 7700 years old. The size of the lava flow is not known exactly because it is extensively covered by younger lava flows but is thought to be ~5 km^3. The lava fields of Eldgjá were produced in a large fissure eruption in 934 AD. These are the lava fields of Landbrot, Meðalland and Álftaver originating from different segments of the Eldgjá fissure. Different parts of the lava fields were produced during different stages of the eruption. Total volume of the lava flow is ~18 km^3 (Larsen, 2000; 2010; Thordarsson et al., 2001). Further discussion of the eruption and lava flows is in Chapter 4.3.

Most, if not all, eruptions at Katla central volcano generate jökulhlaups, which escape from the caldera beneath the outlet glaciers Kötlujökull-, Sólheimajökull- and Entujökull glaciers (Björnsson et al., 2000). All jökulhlaups in historical time have emerged from beneath Kötlujökull to the east (Larsen, 2010). Whether it has something to do with the large Eldgjá eruption in 934 AD is not known (Sæmundsson, 1982; Óladóttir et al., 2008). Most Katla eruptions melt through the overlaying ice in a few hours and then become subaerial (Larsen, 2010). The jökulhlaups that develop are a combination of water, ice and volcanic debris and they can occur several times during an eruption. The jökulhlaups that emerge at the start of an eruption are, however, the largest (Larsen, 2010). During the 1918 eruption the jökulhlaup may have peaked at 300.000 m^3/s and the volume of melt water produced was as much as 8 km^3 (Tómasson, 1996). Both Mýrdalssandur and Sólheimasandur sand plains are mostly formed by volcanogenic jökulhlaups from Katla (Larsen, 2010). The evolution of the Mýrdalssandur sand plain will be discussed further in Chapter 4.1.1.

3 Magnetic theory

Magnetism is a phenomena we cannot see or feel directly but it can be observed on a compass (Mussett and Khan, 2000). Mankind has been fascinated by it for thousands of years but it is impossible to be sure when magnetism was first discovered. The Chinese, however, used magnetite rich rocks called loadstones as direction finders as early as in 200 BC (Lowrie, 2007). The first compass used for navigation was however not made until the 12th century in Europe (Reynolds, 1997).

3.1 Basic principles

For over three hundred years the Earth's magnetic field has been thought of originating from a large and somewhat irregular magnet. The field is described to the first order to resemble a dipole field like there is a powerful bar magnet at the center of the Earth. The magnetic poles are approximately aligned with the geographical poles but their position is not fixed and has varied through Earth's history (Mussett and Khan, 2000). In 2010 the tilt between the axis of the dipole field and the rotational axis was 10° but it has varied by several degrees on a time scale of decades and centuries (Maus et al., 2010). The strength of the field varies with location from ~30.000 nT near the magnetic equator and up to ~60.000 nT at the magnetic poles (1 nT = 10^{-9} T) (Finlay et al., 2010). The lines of the magnetic field intersect the Earth's surface at an angle called the magnetic inclination. The field is vertical at the geomagnetic poles but parallel to the surface at the geomagnetic equator (Mussett and Khan, 2000).

The geomagnetic field can be separated into 3 parts. Firstly, the main field which originates from inside the Earth and changes very slowly. Secondly, the small field that is connected to external origins outside the Earth and changes rapidly. And last spatial variations of the main field caused by magnetic anomalies in the Earth's crust (Telford et al., 1990).

The main field is thought to represent ~98% of the total magnetic field. Even though it resembles that of a simple dipole (Fig. 3.1), it is far more complicated (Telford et al., 1990). The main field is generated by convecting currents in the liquid outer core (Hinze et al., 2013). This process is called the geodynamo. It is poorly understood and very complicated. Changes in the convection cause slow and irregular secular changes in the strength and direction of the field. Paleomagnetic data show that the spin of the Earth is coupled with the convective motion of the core where the magnetic field has always been aligned roughly to the Earths spin axis (Telford et al., 1990). Fast and sudden changes in the field have also taken place such as the polarity reversals where the positions of the poles have interchanged. These events have occurred at irregular intervals through Earth's history measured in millions of years. The current configuration of the poles is called normal and the opposite is called reversed (Telford et al., 1990; Mussett and Khan, 2000).

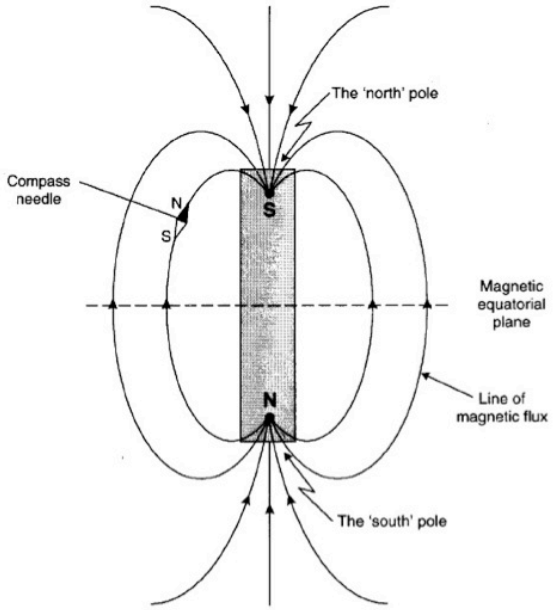

Figure 3.1: The Earth's magnetic field. The field resembles that of a dipole field as if the Earth has a powerful bar magnet at its centre with its south magnetic pole corresponding to the north geographic pole (Reynolds, 1997).

The small field (~2%) or the external magnetic field is generated by electrical currents in the upper atmosphere. It is much more susceptible to time variations than the main field. These variations are 11 year cycles of sunspot activity, solar diurnal- and lunar variations and magnetic storms. The biggest and most rapid variations are the magnetic storms. They can cause disturbances up to 1000 nT and even higher at higher latitudes where they coincide with auroras. The storms are connected to sunspot and solar flare activity and are not meteorological. They are most common in September and March, during the equinox, when solar activity peaks. Solar diurnal variations over 24 hours can be in the range of 30 nT and lunar variations are even smaller. For precise studies these variations can be corrected for by using a reference base station. However, most often they do not need to be corrected for because they are to small to have any effect on the interpretations. However, measurements should not be conducted during magnetic storms because the data will be invalidated due to high disturbances (Telford et al., 1990).

The geomagnetic field has been modeled as and undisturbed theoretical magnetic field. This model is called the International Geomagnetic Reference Field (IGRF) and is often removed from the measured field to show the residual magnetic field of anomalies (Keary and Brooks, 1984). The magnitude of the field is not uniform and increases towards the poles (Telford et al., 1990; Janowski and Sucksdorff, 1996). Figure 3.2 shows the total intensity of the magnetic field at the Earth’s surface in 2010.

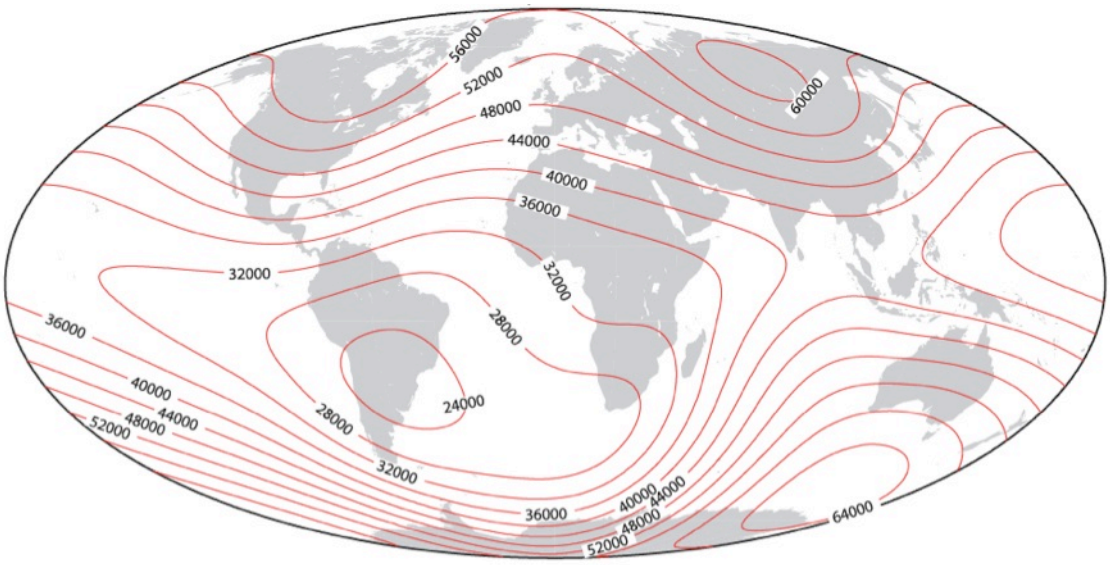

Figure 3.2: Total intensity of the Earth's magnetic field in nT in 2010 (Finlay et al., 2010).

The total magnetic field at any point on the Earth is a vector (F) having both direction and magnitude. The vector (F) has three components a north component (X), an east component (Y) and a vertical component (Z) (Equation 1 and Fig. 3.3). The horizontal intensity (H) is a combination of the X and Y components. The following equation explains the connection between the components of the magnetic field (Janowski and Sucksdorff, 1996).

$$F^2 = X^2 + Y^2 + Z^2 = H^2 + Z^2 \quad (1)$$

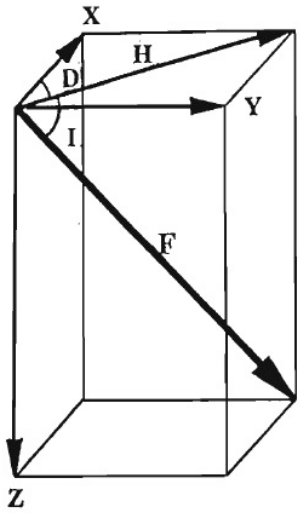

Figure 3.3: Elements of the Earth's magnetic field. F is the total magnetic field, X is the north component, Y is the east component, Z is the vertical component, H is the horizontal component, D is the declination and I is the magnetic inclination (Janowski and Sucksdorff, 1996).

3.2 Magnetization and sources of magnetic anomalies

Magnetized rocks give rise to magnetic fields. The source of magnetization in rocks comes from magnetic atoms in the crystal structure of minerals. Most of the magnetic elements are weakly magnetic meaning that the magnetization does not align perfectly to the magnetic field. With this the material becomes poorly magnetized. However, there are a few elements with a strong magnetization in the direction of the earth's magnetic field for example iron and some of its oxides. Strong magnetization is the principle source of magnetic anomalies with sources in the earth's crust and a large part of magnetic surveying is aimed at mapping out these sources (Mussett and Khan, 2000).

All materials on Earth are magnetic on an atomic scale. Each atom acts as a small dipole because of the spin of its electrons and the orbital path of the electrons around it. Substances can be divided into diamagnetic or paramagnetic according to how they act when placed in a magnetic field (Telford et al., 1990). Diamagnetic substances, such as halite, have all their electrons paired and all of the electron shells are filled. When they are placed in a magnetic field a magnetization is induced. The orbital paths of their electrons rotate and produce a magnetic field opposite to the applied one. The susceptibility of diamagnetic substances is therefore negative and weak. However, paramagnetic substances, such as olivine and pyroxene, have incomplete electron shells with unpaired electrons and its magnetic field is the result of their spin. When put in a magnetic field the dipoles (from the unpaired electrons spin) rotate to produce a field in the same direction as the applied field. This process is retarded by thermal agitation resulting in a weak but positive susceptibility. Paramagnetic substances are of an order of magnitude stronger than diamagnetic ones (Keary and Brooks, 1984; Reynolds et al., 1997). These magnetizations are not relevant for studies of magnetism on Earth because when the substance is taken out of the magnetic field the weak magnetization disappears and the material cannot produce remanence (Mussett and Khan, 2000).

Ferrimagnetism is the most common form of magnetism that produces magnetic anomalies and is the source of almost all the magnetization in any substance on the Earth. In ferrimagnetic substances dipoles are in opposition but the magnetic moments are unequal (Fig. 3.4). Resulting in a combined magnetic moment, which is not zero (Telford et al., 1990; Hinze et al., 2013). The majority of minerals in rocks are diamagnetic or paramagnetic, having little effect on their magnetic characters. There are some minerals that are ferrimagnetic and are important for geological mapping. They occur in titanomagnetite, titanohematite and iron sulfides. The most common magnetic mineral on Earth is magnetite (Fe_3O_4) and it is the principle source of magnetization in rocks. It is commonly the amount of magnetite that controls the magnetization of igneous rocks (Hinze et al., 2013).

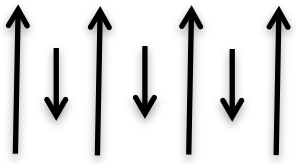

Figure 3.4: Magnetic moments in Ferrimagnetic substances. Magnetic moments in the opposite directions are unequal creating a magnetic moment parallel to the surrounding magnetic field.

Magnetization resulting from ferrimagnetism is further divided into induced and remanent magnetization. The strength of induced magnetization is proportional to the magnitude of the external field and is parallel to it. The proportionality constant between the strength of the external field and the induced field is called magnetic susceptibility (Breiner, 1999). The induced component of the magnetization does not exist when the magnetic field is shut off. The remanent component is present when there is no external field. It adds vectorially to the induced component of the material, which results in a combined total magnetization (Hinze et al., 2013).

Remanent magnetization is the basis for magnetic studies and an important source for magnetic anomalies. It is the magnetization of ferrimagnetic substances that retains the magnetization from a prior magnetic environment. When a remanent magnetized material is taken out of the external magnetic field it does not loose its magnetization. Many types of remanent magnetization have been defined, both on the basis of how the magnetization was formed (called primary magnetization) and through changes that it has gone through during the geological history of the rocks (called secondary magnetization). The sum of primary and secondary magnetization is called natural remanent magnetization (NRM). The most intense and stable form of NRM is thermoremanent magnetization (TRM) produced when the rock is cooled below the Curie temperature, which is around 560°C for magnetite. However, the Curie temperature varies between substances (Hinze et al., 2013). Above this temperature the rock looses its magnetization but below it the atoms of the substance will align to the direction of the current magnetic field and produce a strong remanet magnetization (Mussett and Khan, 2000). The ratio of remanent and induced magnetization is called the Königsberger ratio or Q. In volcanic rocks the remanent magnetization is stronger but in sedimentary rocks the induced magnetization is stronger (Hinze et al., 2013). The remanent magnetization in several basic rocks in Iceland is listed in Table 3.1.

Table 3.1: Remanent magnetization in basic rocks in Iceland (Kristjánsson, 1985; Guðmundsson and Milsom, 1997).

Rock type	**Remanent magnetization (A/m)**
Basalt, Tertiery	3-4
Basalt, Quarternary	~10
Pillow lava	9-17
Present lava flows	10-20
Hyaloclastite	0-1

Iron is the most common magnetic material on Earth, however, not as metallic iron but rather when it is combined with oxygen and sulphur. The magnetism of igneous rocks depends on the concentration of magnetic minerals and the amount of iron present during formation. Igneous rocks make up a large part of the continental and oceanic crust. Thus, they are an important source of magnetization in the Earth. Concentration of magnetic

minerals usually decreases with increasing silica content. However, magnetization of igneous rocks does not only depend on their composition but also their oxidation state, hydrothermal alteration and metamorphism (Hinze et al., 2013). Mafic rocks are often more magnetic than felsic rocks because they usually contain high amounts of magnetite, although some exceptions occurr (Mussett and Khan, 2000).

Sediments such as sand and gravel can contain as much magnetite as crystalline basalts, but the grains in the sediments do not align with the Earth's magnetic field as the gravitational force that controls their settling in rivers and lakes dominates over the much weaker magnetic forces (Hinze et al., 2013). Piles of sediments are therefore essentially non-magnetic. Magnetic anomalies observed over sediments therefore most often reflect magnetic bodies in the subsurface such as igneous rocks, dykes, lava flows or intrusions (Keary and Brooks, 1984). Recent lava flows show magnetization roughly in the direction of the present magnetic field. Thus, they give rise to positive anomalies.

3.3 Survey methods

A variety of instruments have been used over the last 100 years to measure the elements of the geomagnetic field. The fluxgate magnetometer was the first easily portable magnetometer on the scene during World War II for the purpose of detecting submarines. The fluxgate measures the components of the field and its orientation needs to be carefully monitored. Modern instruments often measure only the total magnetic field. They only require coarse orientation and provide instantaneous readings. This has made measuring the magnetic field in air, on land and at sea relatively easy. The most common type of magnetometers is the proton precession magnetometer, used both for surveying work and at magnetic observatories (Keary and Brooks, 1984).

The proton precession magnetometer uses the theory of free precession of protons. The sensor is a bottle filled with a hydrogen rich fluid, often water, kerosene or alcohol (Breiner, 1999). The hydrogen nucleuses act as dipoles, which align parallel to the geomagnetic field (Fig. 3.5 (A)). A current is passed through the coil around the bottle, which produces a magnetic field (F_a) much stronger than the geomagnetic field and in a different direction. The hydrogen atoms align to the induced magnetic field (Fig. 3.5 (B)). The current is then suddenly cut off and the induced magnetic field disappears. The protons realign to the current magnetic field by precessing around it (Fig. 3.5 (C)). The frequency of the precession is directly proportional to the magnetic field intensity.

The proton magnetometer can be used in surveys on land, in air and at sea. Measurements are most commonly done from the air in an airplane or helicopter. Large and remote areas can be measured in a relatively short amount of time and they come to good use when looking for large anomalies such as large igneous intrusions or major faults. However, when looking for smaller anomalies such as dykes, intrusions or lava flows ground magnetic surveys give better and more precise data (Telford et al., 1990).

Ground magnetic surveys are used when looking for shorter wavelength anomalies due to small or shallow sources. They are mostly performed over small areas where profiles are measured in grids. For the surveyor it is important to avoid wearing any metallic objects such as compasses, belt buckles, jewelry or phones. Metallic objects such as railways, cars and fences at the survey site also affect the measurements. Before starting a ground magnetic survey a grid or profile layout must be prepared. The profiles must lie somewhat

perpendicular to the trend of the studied anomaly (Keary and Brooks, 1984). The coordinates of the survey profiles are nowadays usually uploaded into a handheld GPS device, and the surveyor uses the navigation from the GPS to walk straight along the profiles (Mussett and Khan, 2000).

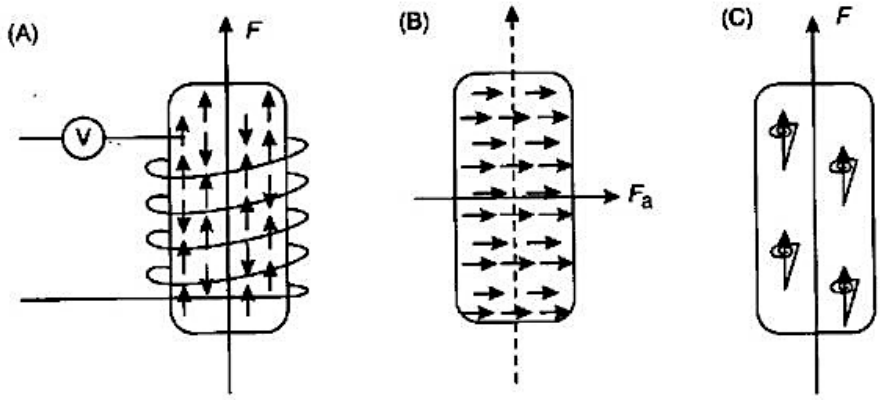

Figure 3.5: The principle of a proton precession magnetometer. A) The sensor is a bottle filled with a hydrogen rich fluid surrounded by a coil and the hydrogen nucleuses align parallel to the magnetic field, B) The nuclei align to the induced magnetic field produced when a current is passed through the coil, C) The nuclei align to the current magnetic field by precessing about it (Reynolds et al., 1997).

3.4 Magnetic anomaly interpretations

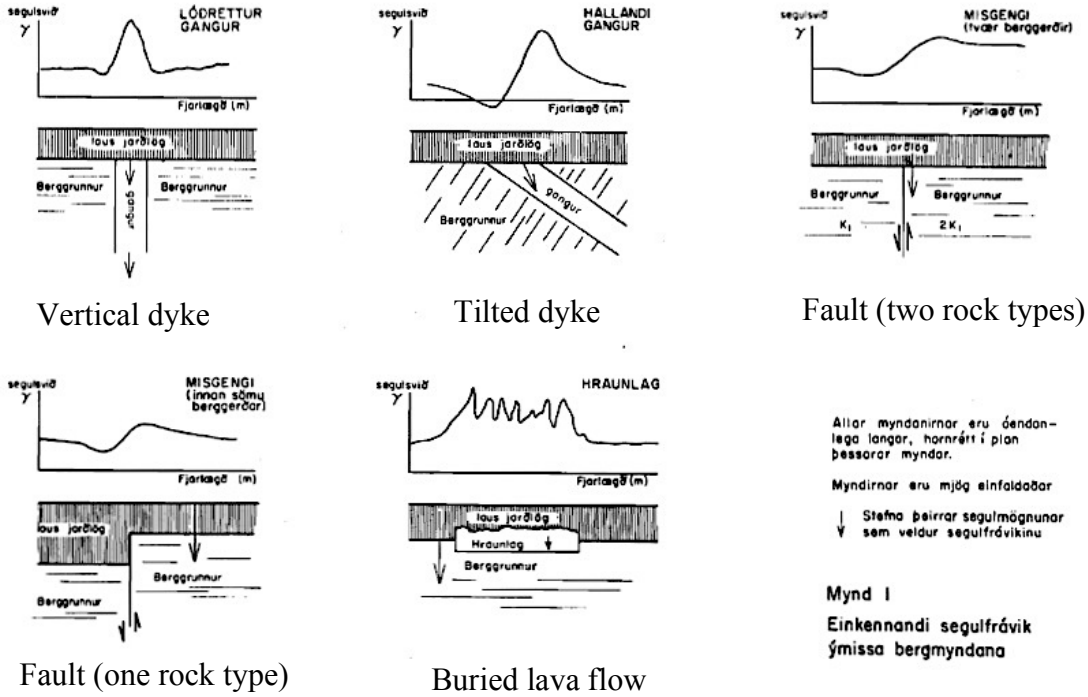

Vertical dyke | Tilted dyke | Fault (two rock types)

Fault (one rock type) | Buried lava flow

Figure 3.6: Magnetic anomalies of buried geological features. The y-axis is the total magnetic field and the x-axis is distance in meter. a) Vertical dyke, b) tilted dyke c) fault with two rock types, d) fault with one rock type, e) buried lava flow (from Georgsson and Jóhannesson, 1979).

The interpretation of magnetic anomalies is similar to the procedures used for gravity anomalies and have similar limitations although being more complex (Keary and Brooks, 1984). The difference lies in the fact that the magnetic method is based on a dipolar field but the gravity method is monopolar. Magnetic anomalies are the sum of attractive and repulsive forces, which complicates the interpretation process. The dipole nature of the magnetic method makes magnetic anomalies sensitive to depth so emphasis has been put on depth estimations in the interpretation processes. Many of the methods used for magnetic interpretations are for restricted use because of limiting assumptions (Hinze et al., 2013).

Although good quality data is needed for high quality interpretations, supplementary information about the subsurface is important. Profile or two dimensional interpretations are often the start of 3D interpretations. However, in most cases it is reasonable to assume a two dimensional body because observations are made along profiles (Hinze et al., 2013). Three dimensional models are also far more complex and mostly used to approximate irregular shapes of the magnetic body (Reynolds, 1997). Examples of total intensity anomalies are presented in Fig. 3.6 for several magnetic bodies. The shape of a magnetic anomaly varies with the dip of the Earth's magnetic field, the shape of the magnetic source and the direction of the magnetization (Milsom, 2003).

3.5 Depth estimations

Estimating the depth to buried magnetic bodies is often the most important goal in magnetic surveying. Many of the methods for depth estimations are based on the maximum gradient of the anomaly, which is the change in anomaly strength in the horizontal direction. The methods vary from simple visual determinations of the gradient to complex computer algorithms (Hinze et al., 2013). The main rule however is that the shallower a body is the sharper and narrower the anomaly (Mussett and Khan, 2000). This can be illustrated by considering Equation (2) for the vertical component of an anomaly from a small vertically magnetized body.

$$Z = \frac{\mu_0 m}{4\pi z^3} \frac{2-(\frac{x}{z})^2}{(1+(\frac{x}{z})^2)^{5/2}} \quad (2)$$

Z is the vertical component of the magnetic body

μ_0 is the magnetic permeability in vacuum, $4\pi \times 10^{-7}$ N/A^2

m is the magnetic dipole moment of the body, given by:

$$m = MV \quad (3)$$

where M is the magnetization in A/m and V is the volume of the body.

z is the depth to the magnetic body

x is the distance along the surface to the axis of the dipole

It is simplest to explain the relationship between the anomaly amplitudes and the depth to the magnetic sources by considering the point directly above the center of the anomaly (x = 0). With x = 0, Equation 2 becomes:

$$Z\,(x=0) = \frac{\mu_0 m}{4\pi z^3}\,\frac{2}{1} = \frac{\mu_0 m}{2\pi}\left(\frac{1}{z^3}\right) = k\left(\frac{1}{z^3}\right) \qquad (4)$$

Where $k = \mu_0 m/2\pi$ is a constant. The amplitude of the anomaly therefore decreases in proportion to the 3rd power of the depth to the magnetic body. The following example explains what happens when the depth to a magnetic source doubles:

$$\frac{Z(z_1)}{Z(z_2)} = \frac{k\left(\frac{1}{z_1^3}\right)}{k\left(\frac{1}{z_2^3}\right)}$$

$$\text{if } z_2 = 2z_1 \text{ then}$$

$$\frac{Z(z_1)}{Z(z_2)} = \left(\frac{2z_1}{z_1}\right)^3 = 2^3 = 8$$

Thus, the amplitude of the anomaly decreases by a factor of 8 when the depth of the magnetic body doubles (Fig. 3.7).

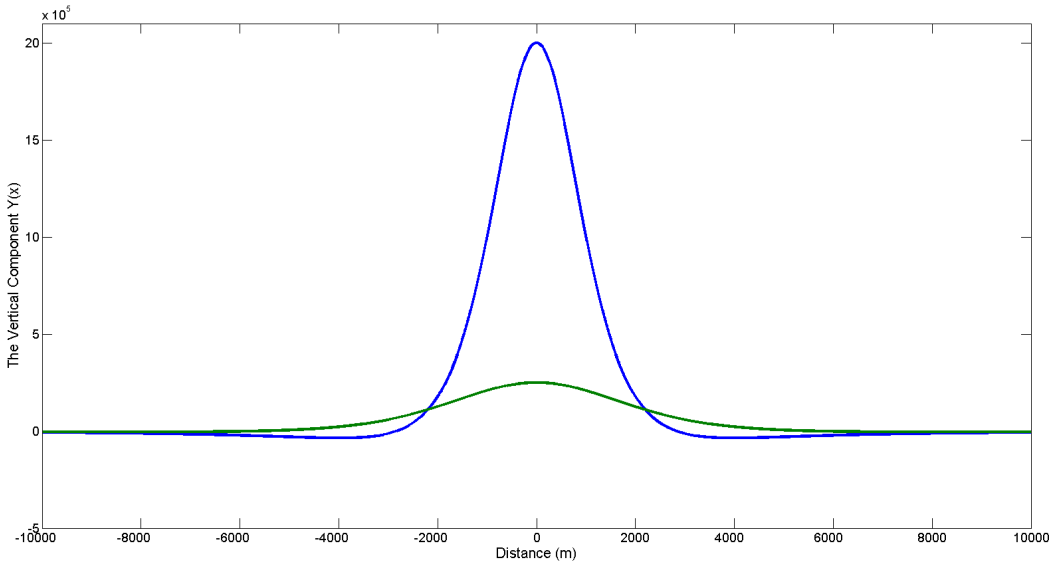

Figure 3.7: Anomaly from a vertically magnetized body. The graph illustrates the relationship between depth to magnetic sources and the amplitude of anomalies. As the sources get deeper the amplitude of the anomaly decreases and it gets wider. The blue anomaly represents a dipole at 2 km depth and the green anomaly represents a dipole at 4 km depth.

Many short cut methods for estimating depth have been constructed and they are often based on a set of simplifying assumptions (Hinze et al., 2013). In this study the depth to the upper surface of the lava flow is estimated using the Peters half slop method (Fig. 3.8) (Peters, 1949). The Peters half slope method is simple to use and gives fairly precise depth estimates and does not require elaborate computations.

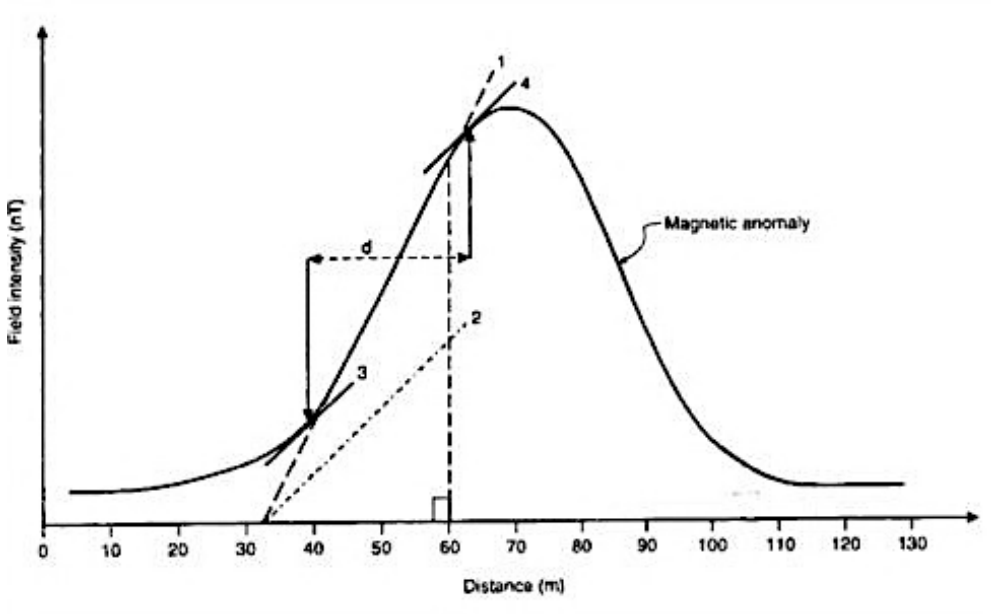

Figure 3.8: Principles of the Peters half slope method (Reynolds, 1997).

The Peters method is performed using the following steps (Fig. 3.8):

1. Draw in the maximum slope on the side of the anomaly.
2. Draw a line with half the maximum slope.
3. & 4. Find the points on the curve where this half slope line is tangent to the curve.
5. The horizontal distance (d) between these points are proportional to the depth (h) to the magnetic body.
6. A proportionality constant is needed. Value of 1.2 applies for thin bodies, 2 is for thick bodies and 1.6 for intermediate bodies. The constant 1.6 is most often used.

The rule can simply be stated as:

$$d = 1.6h \tag{5}$$

This method requires that the anomaly comes from a single magnetic body. This is not always the case and the observed field may be a combination of several sources. However, the rapid attenuation of the field with increased depth implies that the method often works well for a layer of strongly magnetized sources covered by non-magnetic sediments.

4 The Eldgjá lava flow, settings, surveying and results

4.1 Regional setting

Eldgjá is a 75 km long discontinuous fissure in the Katla volcanic system in S-Iceland. The fissure extends southwest to northeast from beneath the glacier of Mýrdalsjökull towards the glacier of Vatnajökull (Larsen, 2000). The Eldgjá eruption is among the largest basaltic flood lava eruptions in the last millennium (Miller, 1989). The exact date and duration of the eruption is not known but the year 934 AD is commonly used (Thorarinsson, 1955; Larsen, 1979; Hammer, 1984; Zielinski et al., 1995). The Book of Settlement written by the Norse settlers that came to Iceland in 870 AD, describes a lava flow, coming from the north destroying farmlands in the south. Tephrochronological studies have also indicated that the eruption took place in the 10^{th} century (Larsen, 1979). A large acidity peak in the Greenland ice core correlates well with the timing of the eruption to be in 934 and indicates that the eruption could have lasted for up to 9 years, from 933 to 941 AD (Hammer, 1984; Zielinski et al., 1995). The fissure opened up in a pre-existing valley or a depression occupied by a river at the time of the eruption. The activity during the eruption was in episodes separated by intervals of low or no volcanic activity (Larsen, 2000; 2010). Each episode started with an explosive phase followed by fire fountaining and an episode of lava effusion (Miller, 1989).

Huge amount of tephra, gas and lava was produced in the eruption, which had a major impact on neighboring areas. Most of the tephra was produced by the subglacial part of the fissure below Öldufellsjökull glacier with dominating explosive phreatomagmatic activity with wide dispersal of tephra. Most of the tephra was carried southeast covering a land area of 20.000 km^2 but the area at sea has not been estimated. The total volume of the tephra has not been estimated because a huge part of it was dispersed to sea but is thought to exceed 6 km^3 (Thordarson et al., 2001; Larsen, 2010). Large amount of lava was erupted producing extensive lava fields in the south. The lava followed rivers and valleys down to the lowlands, forming the lava fields of Álftaver, Meðalland and Landbrot (Fig. 4.1) (Larsen, 2000). The tephra and lava flows have the chemical characteristics of material from Katla or a transitional alkali basalt with high content of iron and titanium (Jakobsson, 1979). The lavas are in some places dominated by rootless cones produced when the lava flowed over wetlands and lakes (Larsen, 2000; 2010). Estimates of the volume of the lava flow has varied during recent decades from 14 km^3 (Miller, 1989) up to ~18.3 km^3 (Thordarson et al., 2001). However, the western part of the Álftaver lava flow is covered by the Mýrdalssandur sand plain (Fig. 4.1) and the volume has thus never been accurately estimated (Larsen, 2010). The most recent volume estimates of ~18.3 km^3 (Thordarson et al., 2001) makes the Eldgjá lava flow one of the largest lava flows on Earth in the last 11 centuries (Larsen, 2010). Comparable in volume to the Laki lava flow (14.7 km^3), produced in 1783 – 1784, covering parts of the Eldgjá lava flow (Thordarson et al., 2003). The most activity was on the ~8 km long fissure closest to Öldufellsjökull glacier which,

produced the Álftaver lava flow (Larsen, 2000; 2010). Kriki hyaloclastite flow deposit is thought to have formed during the Eldgjá eruption. It's situated at the northern margin of the Kötlujökull glacier at Kriki and is extensively cut by rivers. It is a combination of lava, pillow lava, hyaloclastite breccia and hyaloclastite tuff. The edges of the flow deposit are not visible and are buried beneath alluvium from rivers and jökulhlaups (Larsen, 2000).

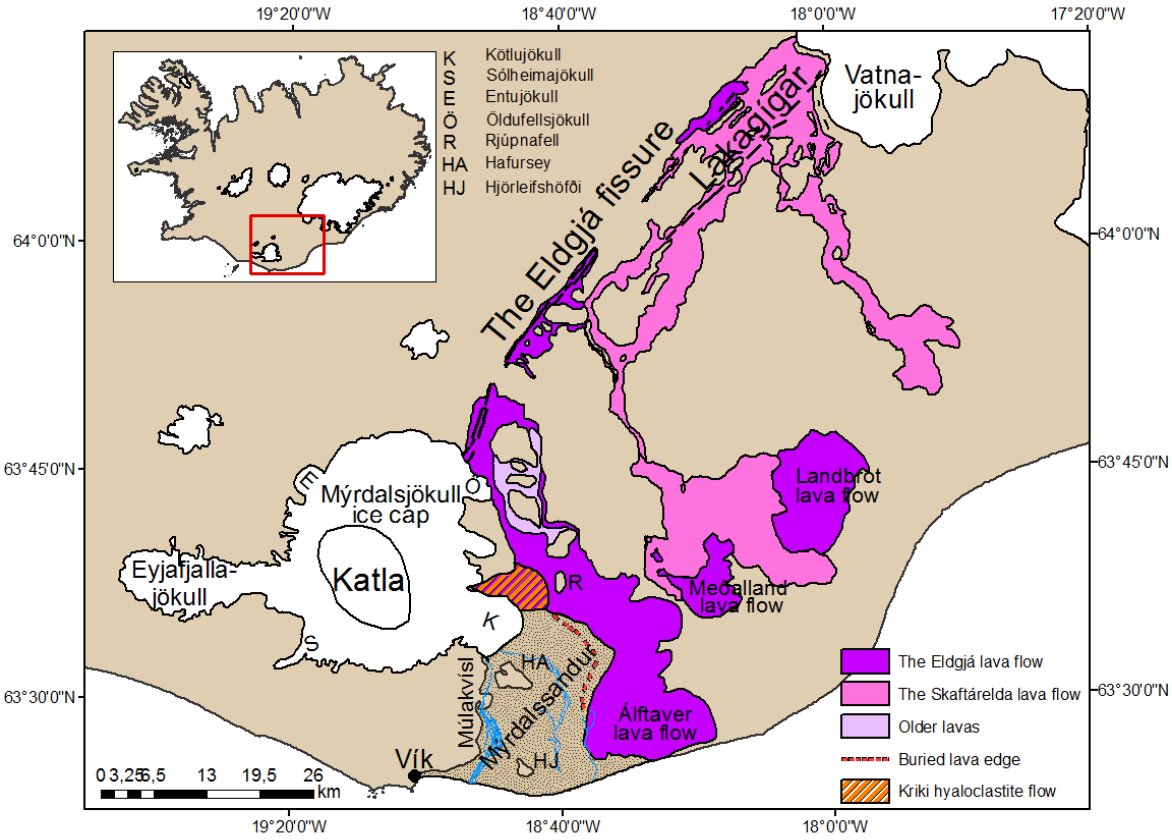

Figure 4.1: The Katla volcanic system. The subaerial part of the Eldgjá fissure and the lava flows from the 934 AD eruption is shown. The exposed parts of older lava flows are shown as well as the Skaftáreldar lava from the 1783-84 Laki eruption. Previously determined edge of the lava flow beneath Mýrdalssandur is marked with discontinuous red line (Larsen, 2000). The outline of the Álftaver lava flow is modified from Larsen (2000). The Meðalland- and Landbrot lava flows and Skaftárelda lava flow is modified from Jóhannesson and Sæmundsson, 1990.

Jökulhlaups did accompany the Eldgjá eruption but their timing and flow paths are only partly known. It's most likely that a jökulhlaup came from beneath Öldufellsjökull glacier. South of Öldufell there is a fan deposit from a jökulhlaup overlain by the Eldgjá tephra, which was deposited during the early stages of the eruption (Larsen, 2010).

The Eldgjá eruption was a major event, not only because of its magnitude but also because of its environmental impact. Huge amount of SO_2 were released into the atmosphere and it is estimated that 220 Megatons went into the atmosphere both through vent and lava flow degassing. This makes the Eldgjá eruption the greatest volcanic pollutant from a flood lava eruption in the last 1100 years exceeding Tambora and the Laki eruptions. About ~79% of the SO_2 was degassed at the vents during the initial explosive stages of each eruptive

period. This affected the climate worldwide with unusually cold winters and crop failure in Europe and Asia (Stothers, 1998; Thordarson et al., 2001; Fei and Zhou, 2006; Larsen, 2010).

4.1.1 Environmental changes at Mýrdalssandur

The southern coast of Iceland has evolved drastically during the Holocene by a combination of glacial, fluvial, volcanic and marine processes (Nummedal et al., 1987). The Mýrdalssandur sand plain has mostly been formed in volcanogenic jökulhlaups from Katla and the environment there has been drastically changed over the past millennium (Thorarinsson, 1975; Jónsson, 1982; Nummedal et al., 1987; Larsen, 2000; 2010). Jökulhlaups are most often shortlived events that disrupt the environment, morphology and sediment patterns of the outwash plain. For example the coastline at Skeiðarársandur has not changed drastically but has stayed fairly stable through the decades. In contrast, the progradation at Mýrdalssandur has been very fast. The sediment deposition from Katla jökulhlaups have extended the coastline of southern Mýrdalssandur significantly and it is considered now to lie 2.2-2.5 km south of its location in 1660 (Fig. 4.2) (Nummedal et al., 1987).

Katla eruptions melt their way through several hundred meters of ice and produce vast amounts of melt water generating the largest floods observed in Iceland (Thorarinsson, 1975; Tómasson, 1996; Larsen, 2000). The largest jökulhlaups carry with them huge amounts of sediments and ice blocks from the glacier. For example estimates of the total sediment volume in the 1918 jökulhlaup ranges from 0.7 to 1.6 km^3 (Tómasson, 1996; Larsen and Ásbjörnsson, 1995). Figure 4.2 shows the impact area of jökulhlaups coming from beneath Kötlujökull. The blue lines indicate estimated location of the jökulhlaup front in hours from the start of an eruption. The large volcanogenic jökulhlaups have occurred about once every 50 years. Very small jökulhlaups (10-100 m^3/s) occur every year and medium sized events (2000-5000 m^3/s) have occurred three times since 1955 (Thorarinsson, 1957; Eliasson et al., 2006; Guðmundsson and Högnadóttir, 2006). These jökulhlaups are a consequence of cauldron drainage due to enhanced geothermal activity and volcanic unrest, increased melting during summer time and high precipitation (Eliasson et al., 2006; Sturkell et al., 2008). The most recent medium sized flood occurred in the summer of 2011. It came from beneath Kötlujökull glacier and flowed down Múlakvísl, destroying the bridge at Highway 1. The flood might have resulted from increased geothermal activity (Galeczka et al., 2014) but a minor subglacial eruption or a shallow dyke intrusion, cannot be ruled out as at least a contributing factor (Guðmundsson and Larsen, 2013). The other medium sized event occurred in 1955 (Thorarinsson, 1957) and in 1999 (Russell et al., 2010).

The environment at Mýrdalsjökull glacier has been altered drastically through time and has significantly changed since the Eldgjá eruption. The lava fields changed the topography, hydrology, utilization potential of the area east of Mýrdalsjökull and the runoff of rivers and jökulhlaups (Larsen, 2000; 2010). Since the Eldgjá eruption large jökulhlaups accompanying eruptions at Katla have only emerged from beneath Kötlujökull glacier (Thorarinsson, 1975). After the Eldgjá eruption in the 10^{th} century the high topography of the Álftaver lava formed a barrier preventing jökulhlaups from flowing to the east. Jökulhlaups that have flowed down Mýrdalssandur since the Eldgjá eruption have been obstructed by the lava field and directed to the south. The sand plain rose with every jökulhlaup until it had reached the same elevation as the lava field. Jökulhlaups were then

able to flow to the east over the lava field, burying it in alluvium (Larsen, 2000; 2010). Today, the Álftaver lava is partially buried beneath Mýrdalssandur and the exact location of its edge is not known. As a result it has not been possible to estimate its volume with accuracy. With time and continued volcanic activity and jökulhlaups from Katla, progressively larger parts of the lava flow will be buried beneath Mýrdalssandur.

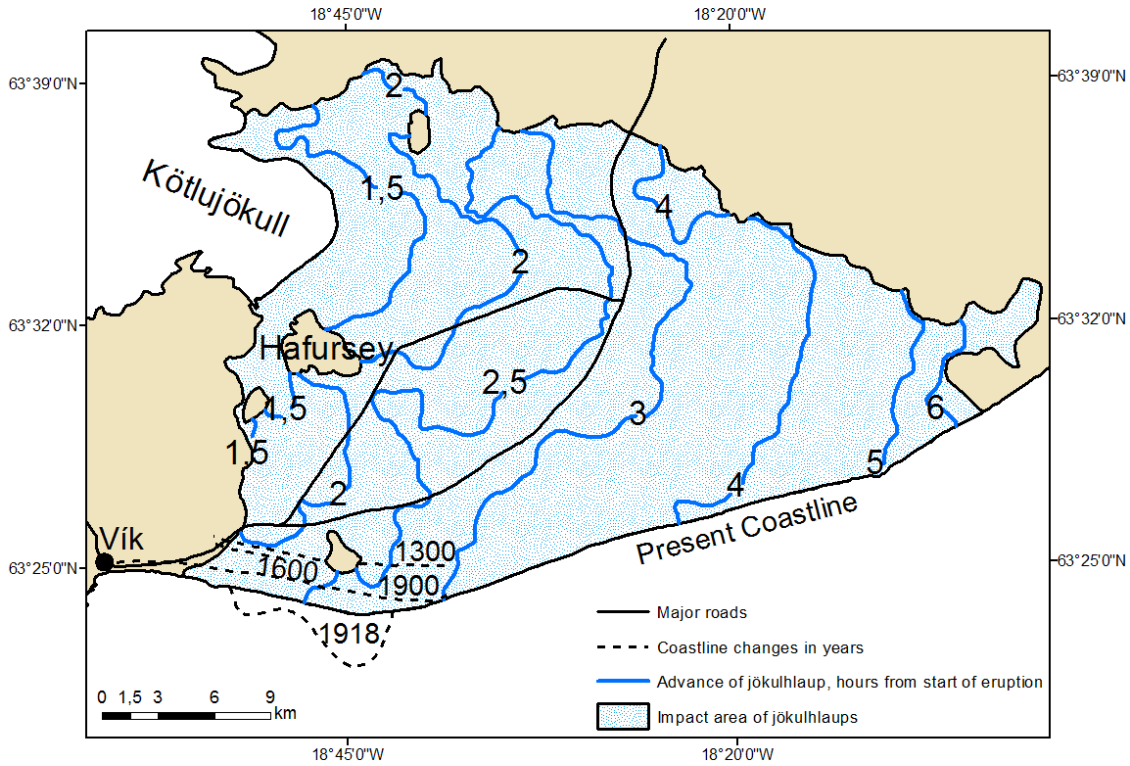

Figure 4.2: Impact area of jökulhlaups coming from beneath Kötlujökull. Blue lines show the advances of the jökulhlaups in hours from the start of the eruption (Guðmundsson et al., 2008). Coastline changes are shown with dashed lines where the correlated year is shown above it Nummedal et al., 1987.

4.1.2 Previous research of sand thickness on Mýrdalssandur

In 1978 geoelectrical soundings and seismic surveys were conducted at Mýrdalssandur by the National Energy Authority (Fig. 4.3). The aim of the research was to map the thickness of the pumice-rich sediments that form Mýrdalssandur. The bedrock below the sediments was found to be relatively flat, 10 – 25 m below sea level. The total sediment thickness above the bedrock was revealed to be up to 60 m in the area around Hjörleifshöfði increasing towards Hafursey being up to 122 m there (Thórarinsson and Guðmundsson, 1979).

Since 2009 a total of 29 research boreholes have been drilled into the Eldgjá lava flow at Mýrdalssandur for the purpose of estimating possibilities for rock quarrying. The rocks were planned to be used in marine erosion protection at the village of Vík and for eriosonal protection at the Múlakvísl river. The area east of Dýralækir was first explored with 11 boreholes studied. In 2011 the Icelandic road and coastal administration looked at the

possibility of quarries in several places at the Eldgjá lava flow. During the spring of 2012 quarrying possibilities were again looked at for erosional protection at the new bridge over Múlakvísl (Vegagerðin, 2013) resulting in an experimental quarry in area B (Fig. 4.3). The experimental boreholes have revealed that the thickness of the lava flow in an area extending from Highway 1 down to the quarry area (Fig. 4.3) is at maximum 25 m. Areas A and C (Fig. 4.3) are the only areas where the drill went through the lava flow showing its upper and lower surfaces, which revealed the thickness of the lava flow beaing 18-25 m. The uppermost 6-10 m is porous while the lower 15-18 m is made up of dense basalt, which lies mostly in 2-3 zones. This is consistent with the lava having been emplaced as a series of lobes. The lower border of the lava flow does not show any evidence for sudden cooling due to contact with water. It now lies 8 m below sea level indicating that the lava flowed over dry sand and that the area has subsided due to excess loading of the lava flows. In the summer of 2012 further experimental quarrying was inspected in area B (Vegagerðin, 2013).

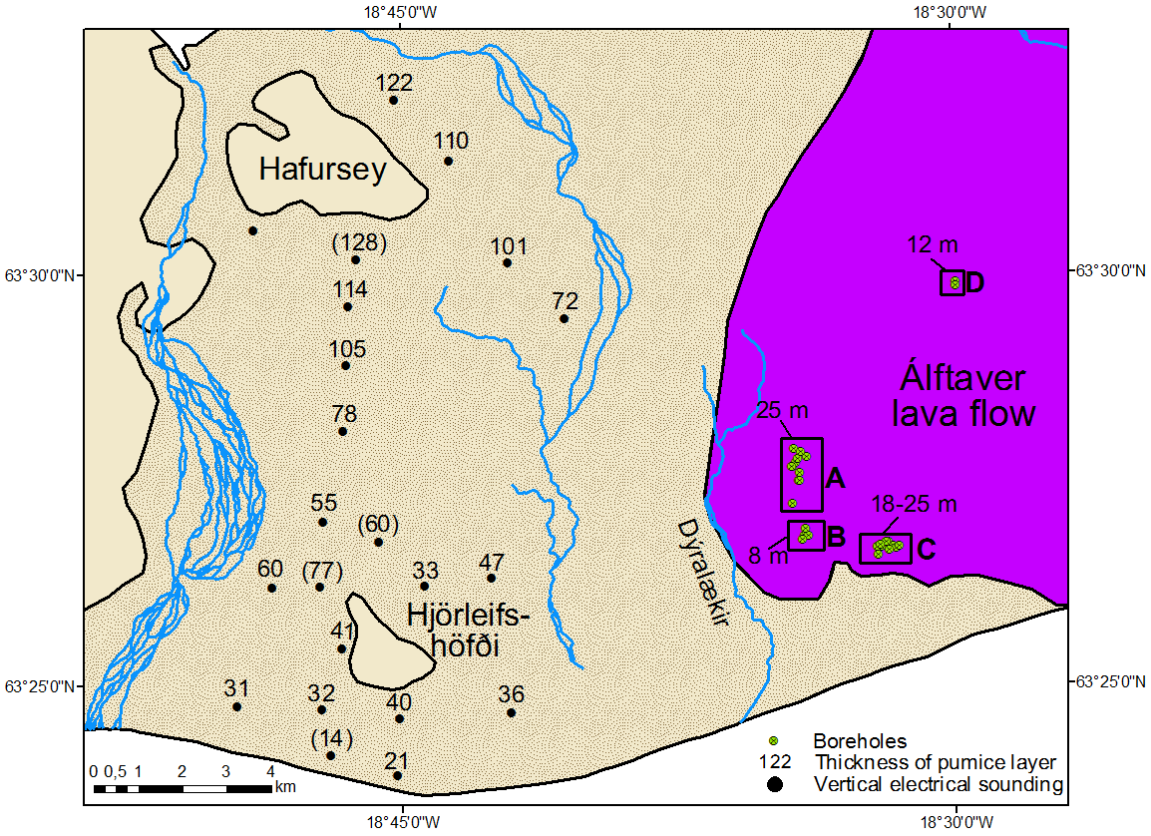

Figure 4.3: Previous research of sand thickness on Mýrdalssandur. Geoelectrical soundings and research boreholes are marked with a black dot and a green dot respectively. The thickness of the sand in meters is shown above each sounding. The thickness of the Eldgjá lava flow is given for each area marked A, B, C and D. Modified from Thórarinsson and Guðmundsson (1979) & Vegagerðin (2013).

4.2 Methods

In total 14 magnetic profiles were measured across the area where the western margin of the Álftaver lava flow is expected to be located (Fig. 4.4) with an automatic proton

magnetometer. The magnetometer used was GSM-19T v7.0. It has a <0.1 nT sensitivity, 0.01 nT resolution (number of significant digits on the display) and 1 nT absolute accuracy over it's full temperature range (GEM systems, 2010). Measurements were done in predetermined, 1-15 km long profiles, lying almost perpendicular to the expected edge of the lava flow. The total length of the profiles is ~75 km. Most of the profiles were measured on foot. However, the western most parts of profiles 4, 5 and 8, of a total length of ~24 km, were measured over snow with a car pulling a sled on which the magnetometer was mounted. The distance between the car and the magnetometer was ~4 m. A handheld GPS instrument was used for positioning of the profiles but the magnetometer has an inbuilt GPS with differential correction yielding position accuracy of about 1 m. Measurements were done at 2 sec intervals where the total magnetic field in nT and the GPS position was measured. The setup of the magnetometer during the walking part of the study is shown in Fig. 4.5. The setup of the magnetometer during the part measured by car is shown in Fig. 4.6. The sensor was always placed 2 m above the surface with the GPS antenna one meter higher at 3 m height.

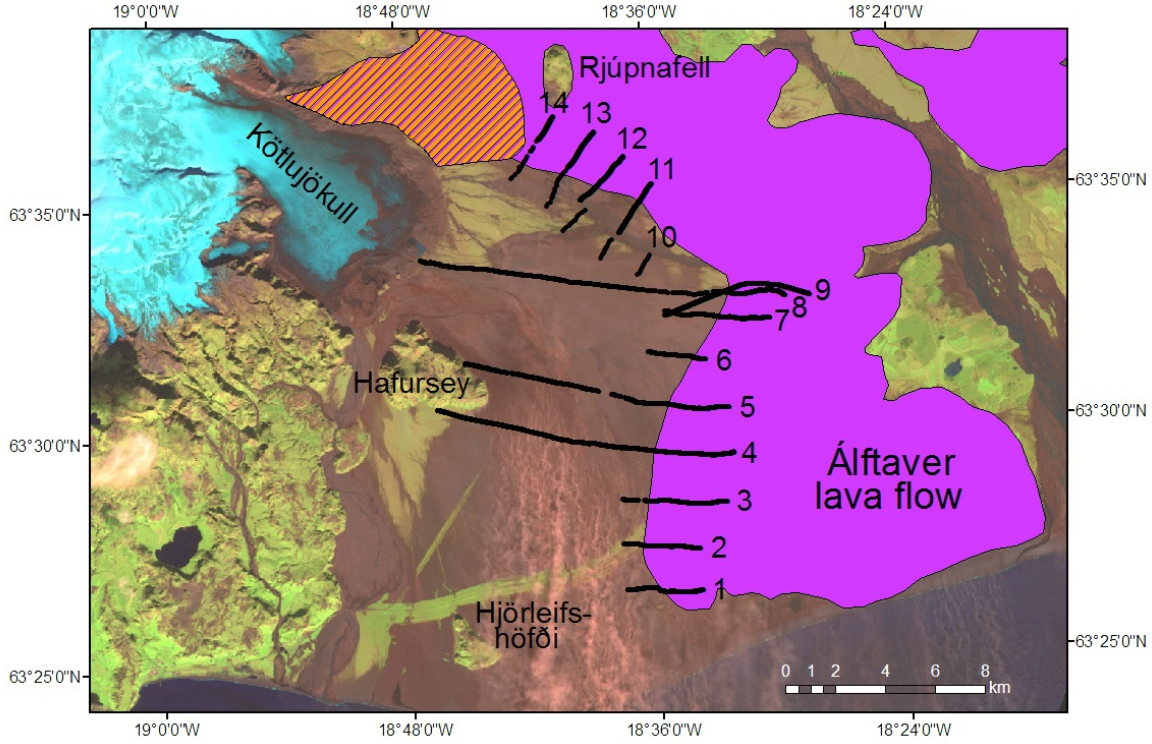

Figure 4.4: Magnetic profile layout at Mýrdalssandur. Profiles are marked 1-14. The Álftaver lava flow is modified from Larsen (2000). Satellite image is a Landsat 8 image from august 2013 (United States Geological Survey, 2014).

The portion of the measurements that were done on foot took a total of 8 days and was measured in June, September and October of 2013. The part measured by car was done during one day in March of 2014. Days for measurements were carefully chosen. Most important was to avoid magnetic storms (100-1000 nT) and days with high magnetic variations (Geophysical Institute, 2014). Secondly it was important to choose days with fairly good weather since the study area is an outwash plain and in very wet weathers the rivers can be impossible to cross by foot. Corrections for diurnal and lunar variations (<100 nT) were not expected to be needed, as the anomalies studied are orders of

magnitude larger. Topography corrections were not needed as the survey area is flat and without appreciable topography that can give rise to anomalies. No significant changes were observed at Leirvogur Magnetic Observatory during the measurements confirming that no corrections were needed (Segulmælingastöðin í Leirvogi, 2014). Data gaps are visible on some profiles because no measurements were done across rivers that were too deep or too fast flowing.

The principal aim of the survey was to identify depth changes to magnetic sources. After the profiles had been plotted segments of individual profiles, with similar spacing of amplitudes (anomaly spatial frequency) and anomaly amplitude, were identified. Spatial frequency changes were identified visually across the profiles but they are directly related to the depth to magnetic sources. The changes were first and foremost used to identify the edge of the Eldgjá lava flow beneath Mýrdalssandur. Secondly to identify ledges on the lava flow where it is thinning outwards to the edge. The Peters half slope method was used to estimate the depth to the magnetic source.

Cross-section modeling of profile 4 was done in Grapher to illustrate the subsurface of Mýrdalssandur sand plain. Profile layout and mapping of the lava flow was done in ArcGIS, using background information from geological maps (Jóhannesson and Sæmundsson, 1990), aerial photographs (Loftmyndir ehf) and Landsat 8 satellite images from USGS Earth Explorer (United States geological survey, 2013). The newly defined edge according to the magnetic measurements was used to re-estimate the volume of the lava flow. It was compared with earlier volume estimates based on older, lava edge locations (Larsen, 2010).

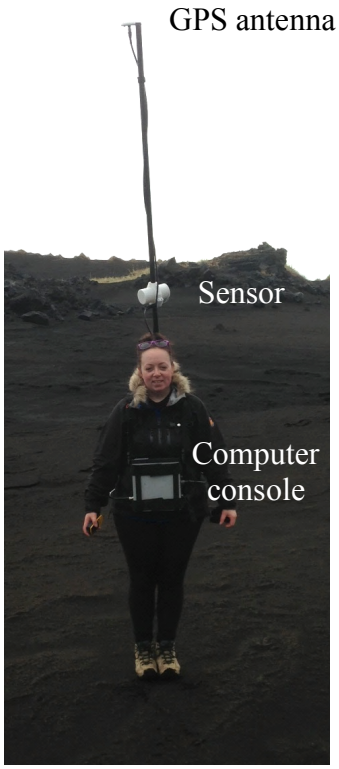

Figure 4.5: Set up of magnetometer during measurements by foot.

Figure 4.6: Set up of magnetometer during measurements by car.

4.3 Results

4.3.1 Magnetic interpretations and depth estimations

Each profile was plotted as distance (m) vs. total magnetic field (nT). All profiles have the same scale for the total magnetic field (y-axis) or 46.000-59.000 nT. The distance (x-axis) varies between profiles but for consistency the distance is the same for all profiles on the same figure. Gaps in data on the profiles are marked with a double arrow. The profiles are separated into sections of changing spatial frequency marked with numbers referenced to numbers in text. The Peters half slope method was used on ca. 6 anomalies in every 1000 m of each profile, the number depending on useable number of anomalies in each profile and avoiding anomalies effected by composite sources. The height of the sensor (2 m) has been subtracted from the depths and they are thus given relative to the surface. Identification of the lava flow on the surface was done in the field, on aerial photographs and satellite images. For location of profiles see Fig. 4.4.

Profile 1
Profile 1 (Fig. 4.7) can be divided into three sections with different spatial frequencies.

1. 0 – 1250 m: Depth estimations indicate sources at 5 – 11 m depth. Visually the anomalies in this section are narrower than in section two. The section ends with a small data gap due to Dýrlækir river that was to fast flowing and couldn't be crossed by foot.

2. 1250 – 2000 m: Anomalies in this section get smoother, however, their amplitude is slightly higher than in section 1. Depth estimates indicate sources at 2 – 9 m depth.

3. 2000 – 3100 m: The section shows narrower anomalies with higher amplitudes than in section two indicating shallower sources, which are estimated to be at 1 – 9 m depth.

The spatial frequency changes observed across the profile cannot be considered a possible lava edge and thus it most likely lies west of the profile. The spatial frequency change between section 1 and 2 can be reflecting a lava ledge.

Profile 2
In profile 2 (Fig. 4.7) there are four sections with different spatial frequencies.

1. 0 – 1400 m: The section shows smooth anomalies, which do not have high amplitudes indicating deep sources. Depth estimations suggest sources at 2 – 12 m depth. A data gap is visible at Dýralækir River, which was too fast flowing to be crossed. The section ends at a big spatial frequency change.

2. 1400 – 1650 m: The anomalies get much narrower than in section 1 and their amplitudes get higher. This indicates a sudden decrease in depth to magnetic sources. The Peters method suggests sources at 1 – 11 m depth.

3. 1650 – 2600 m: In this section the lava flow is at very shallow depth as indicated by the narrowing anomalies and their higher amplitudes. The depth was estimated to be 0 – 2 m, which is as expected since the lava is sticking out of the sand in some places in this section.

4. 2600 m – end: Here the magnetometer is measuring the lava flow on the surface. However, anomalies have lower amplitude compared to section four.

Across the profile the sources get shallower to the east until it is being measured on the surface in section 4. However, no lava edge was identified on the profile indicating that the edge lies to the west of the profile. A lava ledge is possibly located between section 1 and 2 where the narrowness and anomaly amplitude increases significantly.

Profile 3
On profile 3 (Fig. 4.7) there are four sections of different spatial frequencies

1. 0 – 600 m: The section shows smooth anomalies indicative of deep sources. The depth to the sources is 6 – 11 m. The section ends at a data gap at 600 m at the Dýralækir River, which couldn't be crossed by foot.

2. 600 – 2050 m: The anomalies in this section get significantly narrower as well as their amplitude increases. The sources gets shallower or to 2 – 8 m depth.

3. 2050 – 3700 m: In this section there is a slight increase in frequency of the anomalies and they also get narrower but their amplitude does not change. The depth to the sources is 0 – 5 m depth.

4. 3700 m – end: The lava flow is being measured on the surface in this section. Amplitude of the anomalies get slightly higher.

A lava edge is not visible on this profile and it most likely lies to the west of the profile. However, a lava ledge lies at Dýralækir River between section 1 and 2. The overall profile shows an increase in amplitude and a decrease in depth to magnetic sources to the east until the lava flow is visible on the surface in section 4.

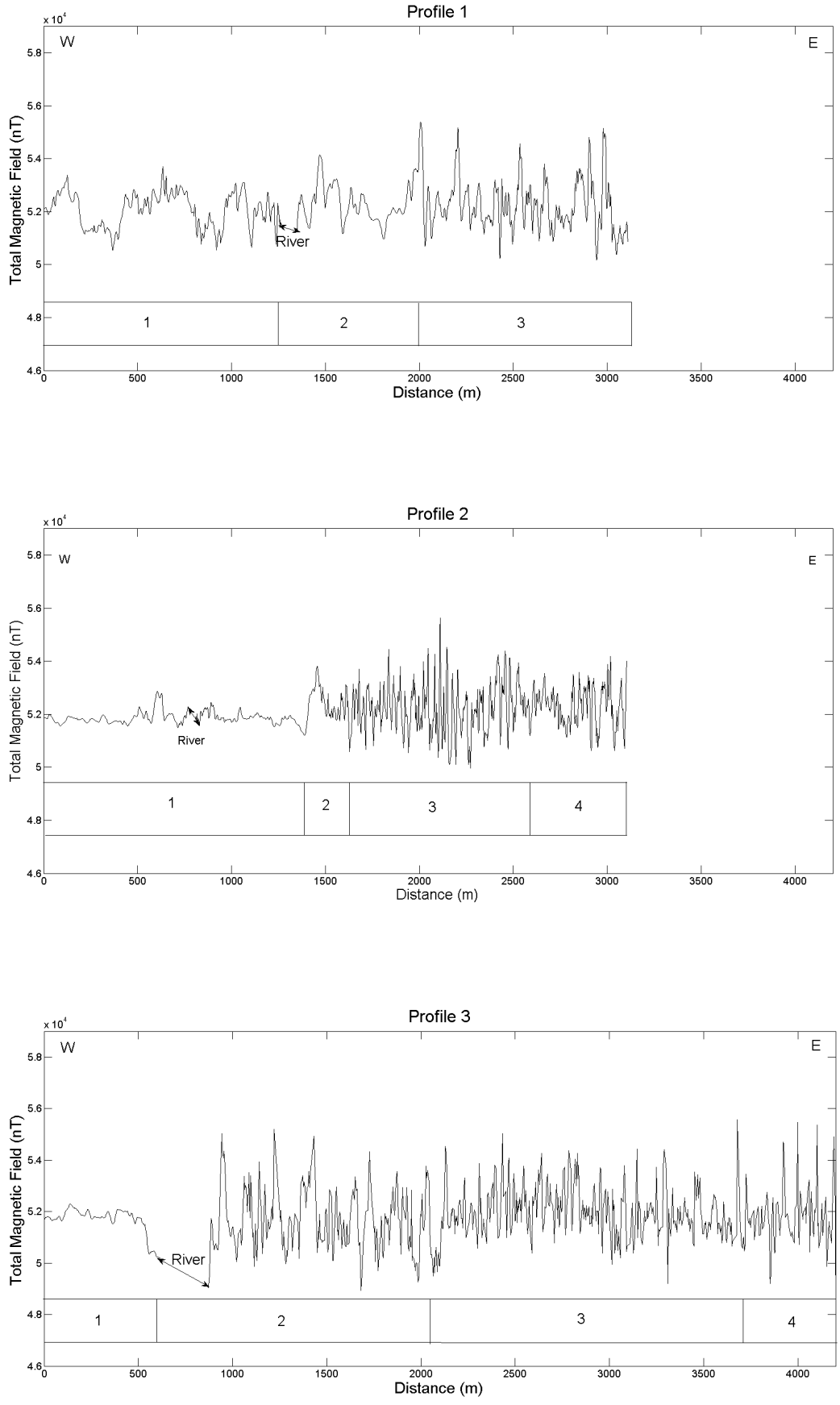

Figure 4.7: Magnetic measurements of profiles 1, 2 and 3.

Profile 4
Profile 4 (Fig. 4.8) goes across Mýrdalssandur from Hafursey in the west over the visible lava edge in the east. It can be divided into six sections with changing spatial frequencies.

1. 0 – 1800 m: Anomalies in this section are very smooth and wide indicating very deep sources. The depth to the sources is 110 – 160 m. These anomalies could be related to the Hafursey hyaloclastite mountain.

2. 1800 – 7000 m: This section shows hardly any anomalies, however, a couple of anomalies at the first three thousand meters are observed. They are wide and smooth indicating a very deep source. The depth to the sources is estimated to be ~250 – 370 m, which is much deeper than on profiles 5 and 8 on central Mýrdalssandur. The excessive depth is probably connected to a hyaloclastite bedrock, which lowers the magnetic field due to its low remanenet magnetization (Table 3.1).

3. 7000 – 8000 m: The section starts with the reappearance of significant anomalies, which get narrower and their amplitude gets higher. The Peters method suggests sources at 10 – 30 m depth. This is a sudden and very significant decrease in depth to magnetic sources indicative of a shallow buried object.

4. 8000 – 9000 m: Here, anomalies get narrower and their amplitude increases. The depth decreases to 2 – 10 m.

5. 9000 – 11000 m: This section shows again an increase in anomaly amplitude, however, they do not particularly get much narrower. At ca. 9500 m a large anomaly reaching 60.177 nT is seen. It is not known what is causing the anomaly but it could be coming from a big rock, a buried magnetic object or it could simply be a magnetic disturbance. The depth to the magnetic sources in this section is 0 – 2 m. Lava nibs can be seen sticking out of the sand in this section.

6. 11000 m – end: The end of the profile is the lava flow on the surface. Here the amplitude of the anomalies is higher than in section 5.

The magnetic field observed indicates a lava edge at 7000 m between section 2 and 3 seen in the sudden and significant decrease in depth to magnetic sources. A lava ledge is then observed at 8000 m between sections 3 and 4 where the depth goes from 10 – 2 m. The profile shows both evidence of deep magnetic sources in the first two sections and in the following four sections shallow magnetic sources are being measured until the lava flow is being measured on the surface in section 6.

Profile 5
Profile 5 (Fig. 4.8) lies across Mýrdalssandur from the hills of Hafursey. The profile is devided into three sections according to changes in spatial frequencies.

1. 0 – 6000 m: The anomalies in this section are smooth and wide indicating deep magnetic sources. At the start of the profile the magnetic field is low but increases away from Hafursey. The low magnetic field can be related to Hafursey hyaloclastite mountain (Table 3.1). Depth estimations indicate sources at 103 – 126 m.

2. 6000 – 8000 m: The section starts with several data gaps due to some failure in the magnetometer. The anomalies however get narrower and their amplitude gets higher

indicating shallower sources. The depth to the sources is 18 – 26 m. The sudden decrease in depth is suggesting shallow magnetic sources. The exact location cannot be determined due to the gaps in data.

3. 8000 m – end: Here the anomalies get much narrower and their amplitude increases. The depth is 4 – 10 m but lies most likely very close to the surface where lava nibs are seen sticking out of the sand. The visible lava flow lies to the east of the profile.

The sudden decrease in depth between section 1 and 2 is reflecting the edge of a buried lava flow. The depth to the lava edge in this profile is slightly higher than on central Mýrdalssandur on profiles 4 and 8 probably due to the failure in the magnetometer between sections 1 and 2. The sudden decrease in depth between section 2 and 3 is related to a lava ledge.

Profile 8

Profile 8 (Fig. 4.7) is the longest profile or 15000 m long. It starts at the edge of Kötlujökull glacier in the northwest and goes across Mýrdalssandur and over the rootless cones in the southeast. The profile is divided into six sections.

1. 0 – 3000 m: The anomalies in this section are narrower than in section 2, which indicates shallower sources. The Peters method suggests sources at 24 – 52 m.

2. 3000 – 8000 m: The anomalies in this section get smoother indicating deeper sources. The depth to the sources is estimated to be 99 - 110 m.

3. 8000 – 9000 m: The anomalies get significantly narrower indicating much shallower sources. The depth decreases suddenly to 10 – 27 m.

4. 9000 – 12000 m: Here the anomalies get even narrower as well as their amplitude increases. The depth to the magnetic sources decreases again down to 6 – 15 m.

5. 12000 – 14000 m: This section shows an increase in the anomalies amplitude indicating even shallower sources. Depth estimations suggest sources at 4 – 12 m. The lava flow possible lies very close to the surface where in the next section the rootless cones are being measured on the surface.

6. 14000 m – end: In this section the magnetometer is measuring the rootless cones on the surface. The amplitude of the anomalies increases significantly.

The profile shows how the magnetic field changes across Mýrdalssandur. Section 2 is measuring a deep magnetic source until at 8000 m, where a sudden decrease in depth is visible between section 2 and 3, suggesting a lava edge below the sand. From 8000 m the depth to magnetic sources decreases until the rootless cones are being measured on the surface in section 6. A lava ledge is located at 9000 m.

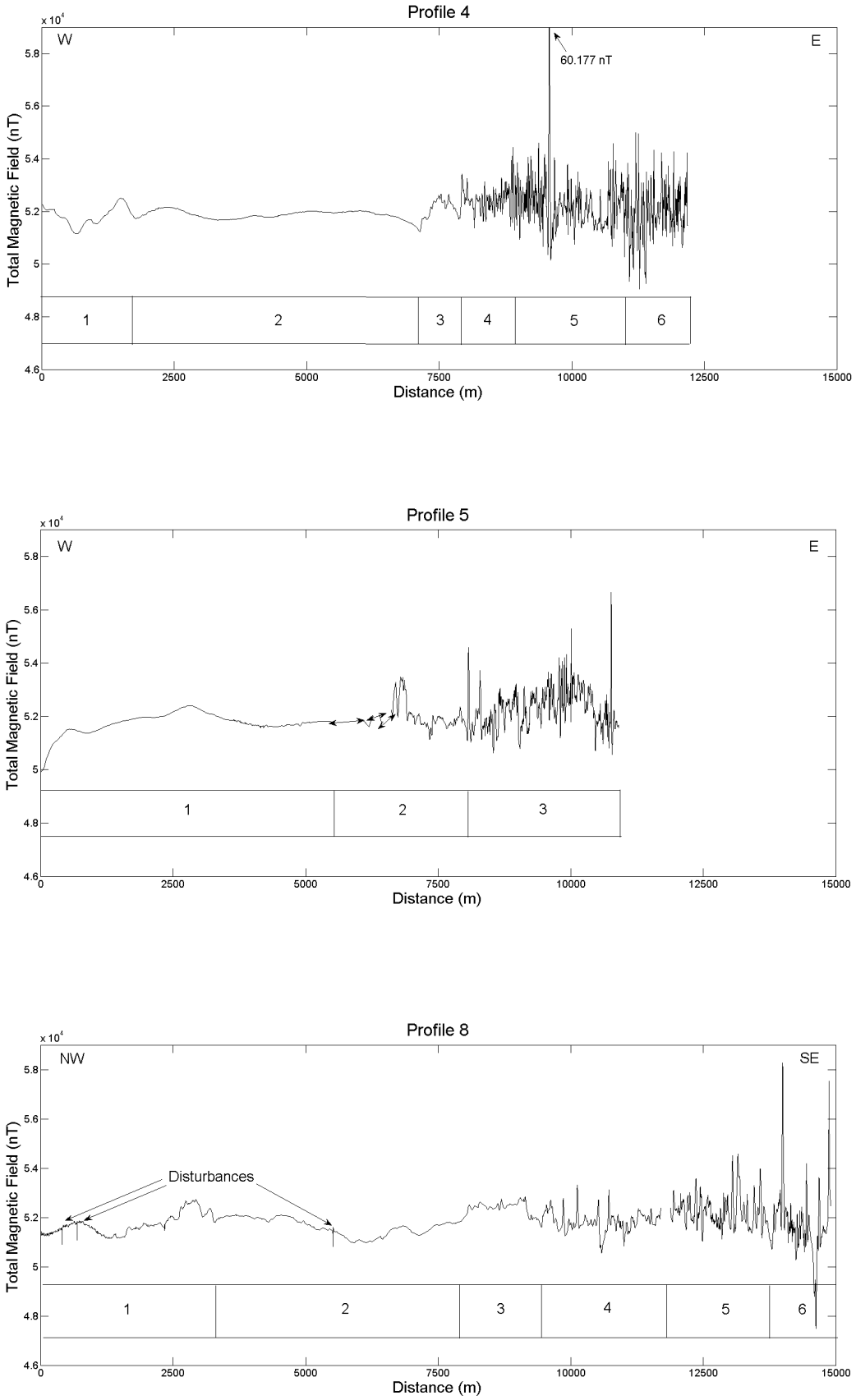

Figure 4.8: Magnetic measurements of profiles 4,5 and 8.

Profile 6
Profile 6 (Fig. 4.9) is 2400 m long and is divided into two sections.

1. 0 – 800 m: The section shows smoother anomalies with lower amplitude than in section 2. Depth estimations indicate sources at 8 – 18 m.

2. 800 m – end: Anomalies in this section get narrower and their amplitude gets higher. The depth decreases slightly to 4 – 14 m.

This profile does not show any evidence of a lava edge suggesting that it is located west of the profile.

Profile 7
Profile 7 (Fig 4.9) shows similar things as profile 6. No significant changes are visible throughout the profile, however the amplitude of anomalies increases slightly to the east. The profile is divided into three sections.

1. 0 – 800 m: Anomalies have lower amplitudes than in section 2. Depth estimates indicate magnetic sources at 11 – 20 m depth.

2. 800 – 2100 m: The section shows an increase in the anomalies amplitude and the depth to the sources decreases to 6 – 13 m.

3. 2100 m – end: The last section also shows an increase in the amplitude of anomalies as well as they get narrower. The depth to the sources in this section is 3 – 11 m.

The profile does not show any evidence of a lava edge thus it most likely lies to the west of the profile.

Profile 9
Profile 9 (Fig. 4.9) was measured on the gravel road that lies across Mýrdalssandur. The profile is divided into three sections.

1. 0 – 1800 m: The anomalies are narrow but smoother than in section 2. Depth estimations suggest sources at 9 – 15 m depth.

2. 1800 – 4100 m: The amplitude of anomalies increases slightly indicating shallowing sources. Depth estimations suggest sources at 4 – 11 m.

3. 4100 m – end: One anomaly extends up to 59.000 nT where the rootless cones are being measured on the surface. However, that changes towards the end of the profile where anomalies get rather wide and their amplitudes decreases, which could be related to the gravel road.

No sudden depth decrease change is visible. However, the first section indicates sources at 9 – 15 m, which is close to the depth to the lava edge in profiles 4 and 5. Suggesting that the lava edge lies slightly more to the west. The magnetic field measured on this profile can, however, be influenced by the gravel road.

Profile 10
Profile 10 (Fig. 4.9) is short or only 900 m because too many deep rivers were on the predetermined profile that couldn't be crossed. The profile however can be divided into two sections. The anomalies get narrower and their amplitude gets slightly higher at 450 m between section 1 and 2. Depth estimations indicate a slight decrease from 9 m to 5-9 m. The profile does not show any indications for a lava edge, which most likely lies southwest of the profile.

Profile 11
Profile 11 (Fig. 4.10) is divided into 5 sections.

1. 0 – 750 m: The section shows very smooth anomalies with high amplitude reflecting deep sources. The depth to magnetic sources is estimated to be 20 – 58 m.

2. 750 – 1700 m: Anomalies change in this section. They get narrower and their amplitude increases indicating shallowing sources. A data gap is observed in this section due to the Þverkvísl River that couldn't be crossed. The depth decreases to 5 – 13 m.

3. 1700 – 2300 m: Anomalies continue to get narrower with higher amplitudes in this section. The depth also continues to decrease, here it goes down to 3 – 10 m.

4. 2300 – 3000 m: The anomalies get narrower in this section but their amplitude decreases slightly. The depth decreases again to 0 – 8 m. The lava flow is close to the surface here because lava nibs are seen sticking out of the sand.

5. 3000 m – end: The anomalies amplitude gets significantly higher because the section is showing measurements on the lava flow on surface.

The profile shows a sudden decrease in depth at 750 m between section 1 and 2 where a lava edge could be located. From there the depth to the sources gets shallower to the northeast until in section 5 where the lava flow is being measured on the surface.

Profile 12
Profile 12 (Fig. 4.10) is divided into 4 sections.

1. 0 – 900 m: In this section the anomalies are wide and smooth. The depth to the sources is 9 – 15 m.

2. 900 – 1800 m: Anomalies in the section get smoother indicating deeper sources. The Peters method yields 18 – 28 m depth.

3. 1800 – 2200 m: Here anomalies get narrower and their amplitude gets higher from section 2 indicating shallowing sources. Depth to the magnetic sources is estimated to be 4 – 8 m.

4. 2200 – 2700 m: Anomalies get narrower and their amplitude increases indicating shallowing sources. Depth to magnetic sources is 2 – 7 m and lies most likely very close to the surface where the lava flow is being measured on the surface in the next section.

4. 2700 m – end: The amplitude increases significantly in this section because here the lava flow is being measured on the surface.

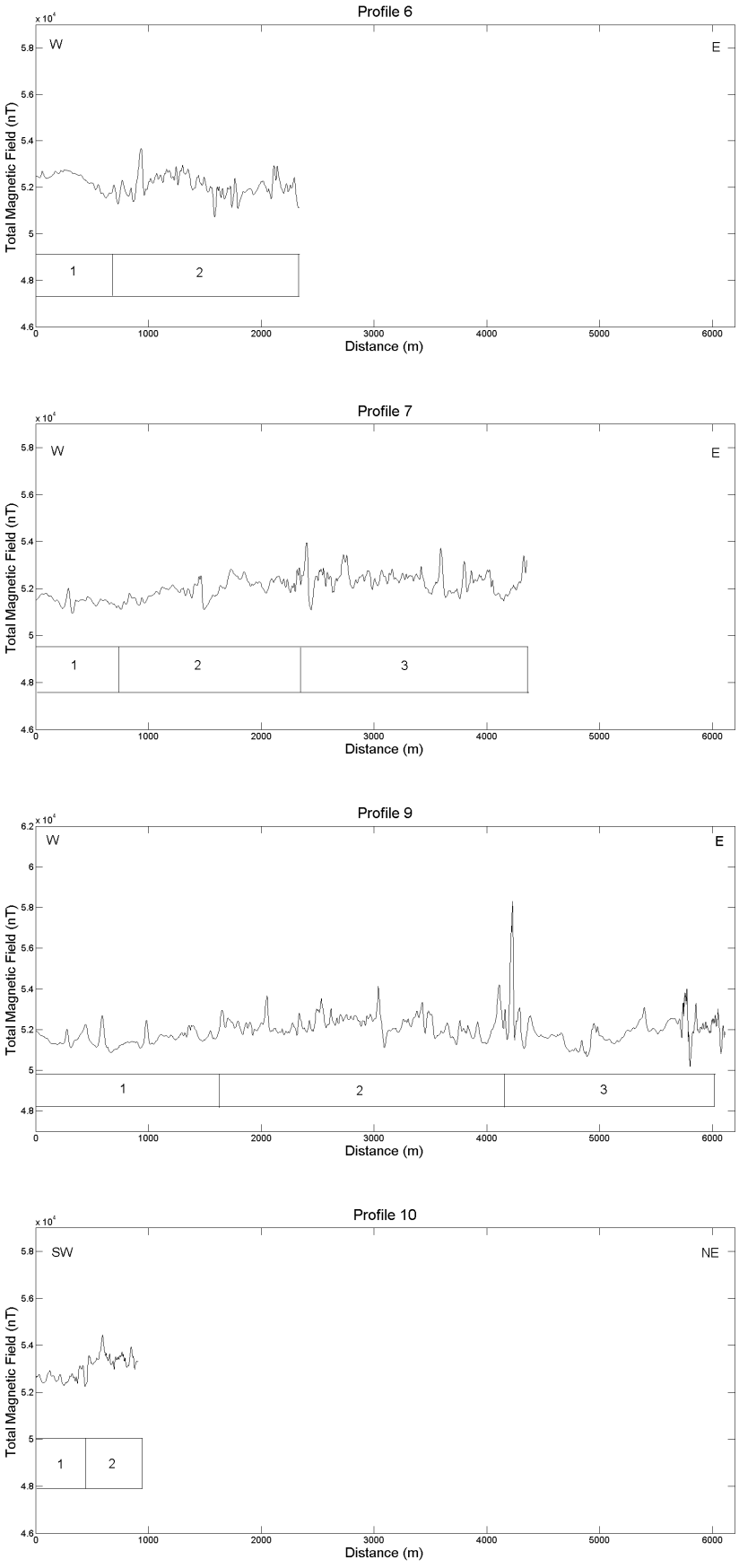

Figure 4.9: Magnetic measurements of profiles 6, 7, 9 and 10.

There are two possible interpretations of this profile. Firstly, that the lava edge is located at 1800 m between sections 2 and 3 because there the anomalies get significantly narrower and the depth decreases abruptly. Secondly, at the beginning of the profile the anomalies could still be reflecting the lava flow below the sand so it is possible that the lava edge is located to the southwest of the profile. The first section could also be reflecting other lava flows below Mýrdalssandur.

Profile 13
Profile 13 (Fig. 4.10) is divided into seven sections.

1. 0 – 250 m: The section shows rather smooth anomalies. The depth to magnetic sources is shallow or 4 – 7 m.

2. 250 – 600 m: Anomalies increase in amplitude and get sharper indicating an even shallower source. Depth estimations suggest sources at 3 – 4 m.

3. 600 – 950 m: Here the amplitude of anomalies decrease significantly indicating much deeper sources. Anomalies get wider and smoother than in section 1 and 2. According to depth estimations the sources lie at 16 – 22 m depth.

4. 950 – 1250 m: The amplitude of the anomalies rise again but stay relatively smooth. Depth to sources is 4 – 12 m.

5. 1250 – 1900 m: The amplitude and sharpness of anomalies increase again indicating even shallower sources, with depth estimations suggesting 1 – 7 m depth.

6. 1900 – 2250 m: The amplitude of the anomalies increases significantly, however, their sharpness decreases a little. Depth estimations reveal sources at 3 – 9 m.

7. 2250 – end: Anomalies get sharper in this section but their amplitude decreases significantly, however, they do increase towards the northeast. Depth estimations reveal shallow sources at 1 – 3 m depth.

The profile does not give any indication of a lava edge. It shows several changes in spatial frequency and depth to magnetic sources. If the profile is measuring the Eldgjá lava flow below the sand the edge most likely lies southwest of the profile. However, the profile could be reflecting several lava different lava flows beneath the surface. It is also possible that the signature on the profile is related to the Kriki hyaloclastite flow below the sand. The alternating depth to magnetic sources could also be related to piles of sediments left behind by the advances of the Kötlujökull glacier.

Profile 14
Profile 14 (Fig. 4.10) is divided into five sections.

1. 0 – 700 m: The first section shows quite smooth anomalies with increasing amplitude to the northeast. The depth to the sources is 4 – 10 m.

2. 700 – 1600 m: The amplitude and narrowness of anomalies increase significantly indicating shallower sources. The depth is 0 – 4 m. The depth is most likely shallow because lava nibs were seen sticking out of the sand.

3. 1600 – 1800 m: Amplitude of anomalies drop and they get slightly wider indicating deeper sources. Depth estimations indicate sources at 3 – 8 m depth.

4. 1800 – 2400 m: The amplitude and narrowness of anomalies drops significantly in this section, which includes a data gap by the Þverkvísl River. Depth to the sources is estimated to be 10 – 22 m.

5. 2400 m – end: In this section the amplitude and narrowness of anomalies increases again and are higher than in section 3. Depth estimations suggest sources at 2 – 10 m.

The profile shows no evidence of a lava edge but is showing alternating increases and decreases in depth to magnetic sources similar to profile 13. If the profile is reflecting the Álftaver lava flow below, its edge lies to the southwest of the profile. It could also be affected by the Kriki hyaloclastite flow or several different lava flows beneath the sand. Another possibility is that the piles of sediments on top of the lava flow left behind by advances of the Kötlujökull glacier.

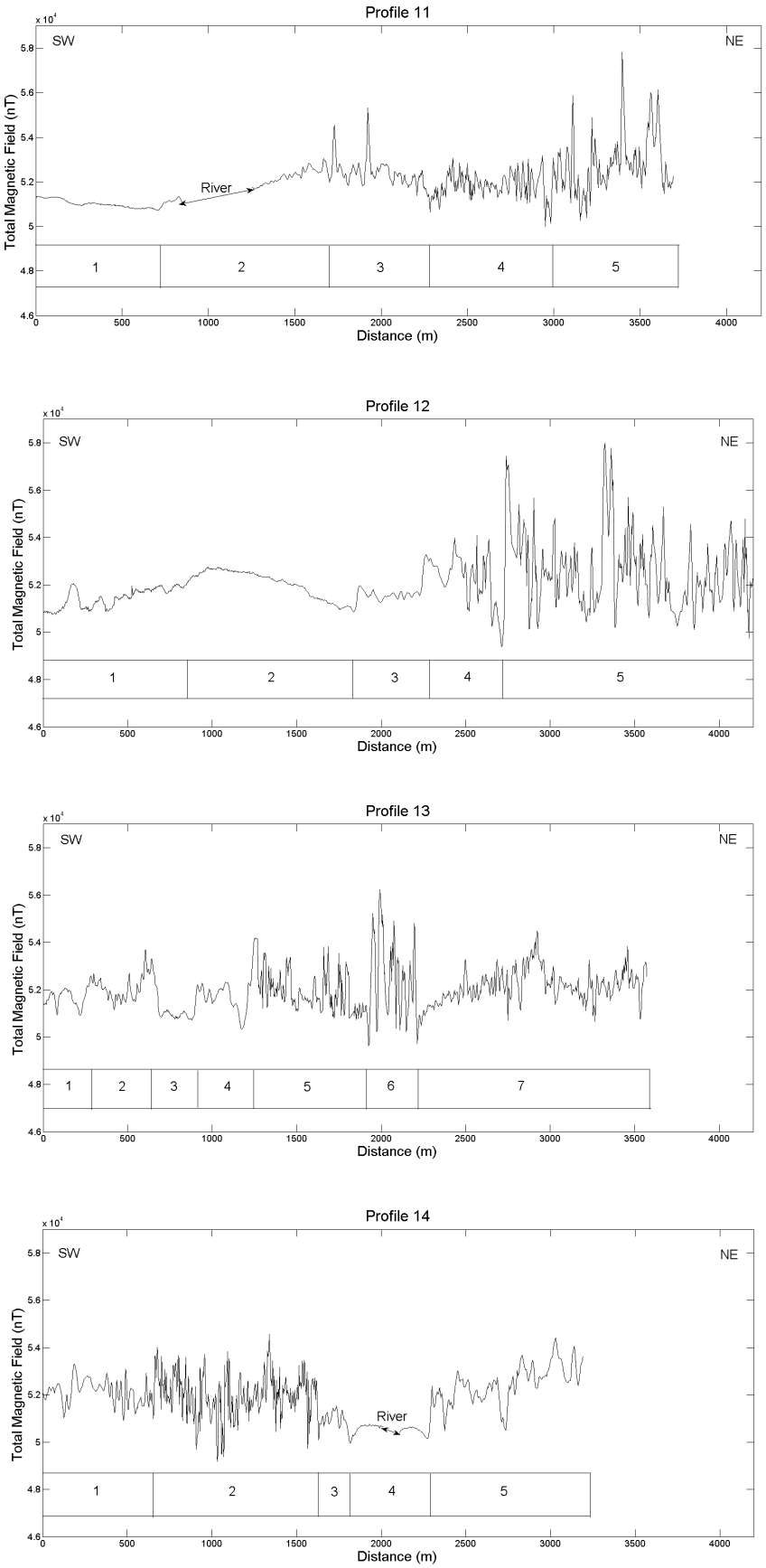

Figure 4.10: Magnetic measurements of profiles 11, 12, 13 and 14.

4.3.2 Mapping of the Eldgjá lava flow

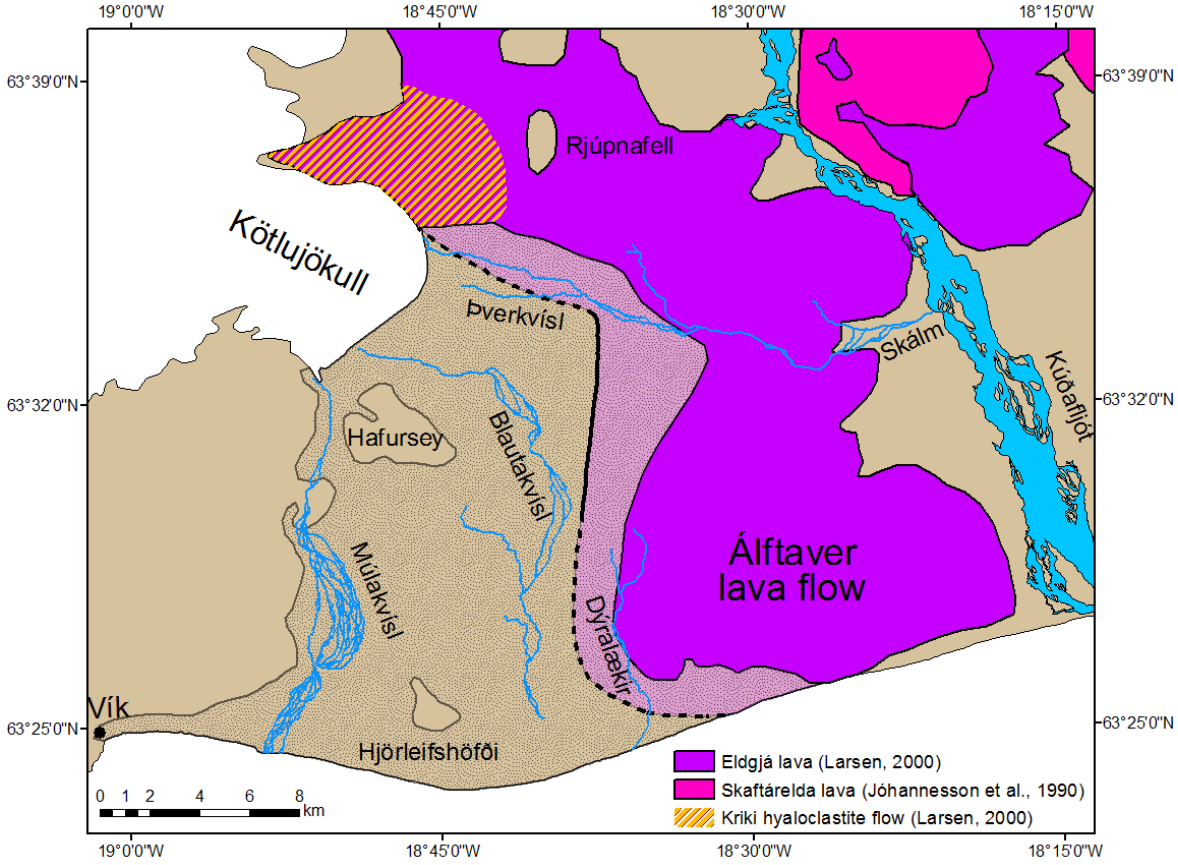

Figure 4.11: The edge of the Eldgjá lava flow beneath Mýrdalssandur. The Álftaver lava flow is modified from Larsen (2000). The part of the lava flow below Mýrdalssandur is shown in light purple. The solid black line is the lava edge beneath Mýrdalssandur according to this study. The dashed black line shows approximately the easternmost possible location of the lava edge.

4.3.3 Area and volume estimates

The location of the Eldgjá lava edge beneath Mýrdalssandur, estimated in this study, was used to re evaluate the area and volume of the Eldgjá lava flow. The area of the lava flow found in this study, which should be added to previous estimates (marked light purple on Fig. 4.11) was calculated with ArcGIS giving 64 km^2.

The thickness of the lava flow is 18 – 25.0 m according to borehole data from Vegagerðin (2013) where the drill went through the lava flow showing both the lower and upper surfaces of the lava flow. Assuming that the lava flow is equally thick towards the edges, the additional volume is estimated (minimum and maximum values):

$$64\ km^2 \times 0.018\ km = 1.1\ km^3$$

$$64\ km^2 \times 0.025\ km = 1.6\ km^3$$

Thus, the additional lava volume that this study adds to previous estimates is 1.4 +/- 0.3 km^3.

4.4 Discussion

Results of the magnetic measurements across Mýrdalssandur and neighboring areas have revealed new information regarding the Eldgjá lava flow. The impact of the results will be discussed in the following sections.

4.4.1 What hides beneath the sand?

The results reveal a shallow magnetic source beneath the eastern part of Mýrdalssandur. The source is considered to be a buried lava flow, which has been found by identifying changes in amplitudes of anomalies, anomaly spacing and depth according to the Peters half slope method. Eight lava flows are known to have originated in the Katla volcanic system and can partly be seen around Mýrdalsjökull glacier (Jóhannesson and Sæmundsson, 1990; Óladóttir et al., 2008. The lava flows that are considered possible to be located in the studied area are the Hólmsá lava flow (7700 years old) and the Eldgjá lava flow (934 AD). The area and volume of the Hólmsá lava flow is not well known because it's mostly covered by the much younger Eldgjá lava flow (Larsen, 2010). The Álftavers lava flow produced in the Eldgjá eruption lies to the east and northeast of the profiles measured in this study (Fig. 4.4). Thus, it is assumed that the magnetic sources being measured beneath eastern Mýrdalssandur is the Eldgjá lava flow with the exception of profiles 13 and 14.

Almost all of the profiles (1-11) indicate a shallow source beneath Mýrdalssandur, which gets shallower towards the east and northeast where the Álftaver lava flow lies on the surface. The only contributing factor to the magnetic anomalies on these profiles is considered to be the Álftaver lava flow. However, because the distribution of the Hólmsá lava flow is not well known it cannot be discarded as having some effect on the profiles.

On profiles 1, 2 and 3 (Fig. 4.7) the lava flow lies at very shallow depth below the surface. The eastern most part of profiles 2 and 3 the Álftaver lava flow lies on the surface. However, the edge of the lava flow is not detected on the profiles and thus must lie west of the profiles (Fig. 4.11).

Profiles 4 and 5 (Fig. 4.8) show the magnetic field across Mýrdalssandur, from the hills of Hafursey in the west to the Álftaver lava flow on the surface in the east. The depth to the lava flow decreases towards the east until it is visible on the surface. The profiles show differences in the magnetic field over a deep and a shallow source, over sediments and a lava flow. The edge of the lava flow is very obvious on these profiles where the anomaly amplitudes get higher and the depth to the magnetic sources drops significantly. The edge is at ~10 – 30 m depth 5 km east of Hafursey (Fig. 4.11 and 4.12). On profile 5 the depth to the lava edge at central Mýrdalssandur is slightly deeper than in other profiles or 18 m. This is most likely due to some confusion in the depth estimations because of the error in the magnetometer during measurements. The depth of section one on profile 4 (110 – 160 m) (Fig. 4.8) is similar to depth estimations to the bedrock below Mýrdalssandur according to vertical electrical soundings (128 m) (Thórarinsson and Guðmundsson, 1979). However, section 2 shows that a magnetic rock lies at 250 m depth, not comparable to the electrical sounding where the bedrock is estimated to be at 101 m depth. The difference may lie in the fact that the bedrock might be made up of hyaloclastite, which has very low remanent magnetization (Table 3.1). Depth estimations on section 1 on profile 5 gives depth to magnetic sources to be 103 – 126 m comparable to results from vertical electrical sounding revealing the bedrock at 110 m depth (Fig. 4.3) (Thórarinsson and Guðmundsson, 1979).

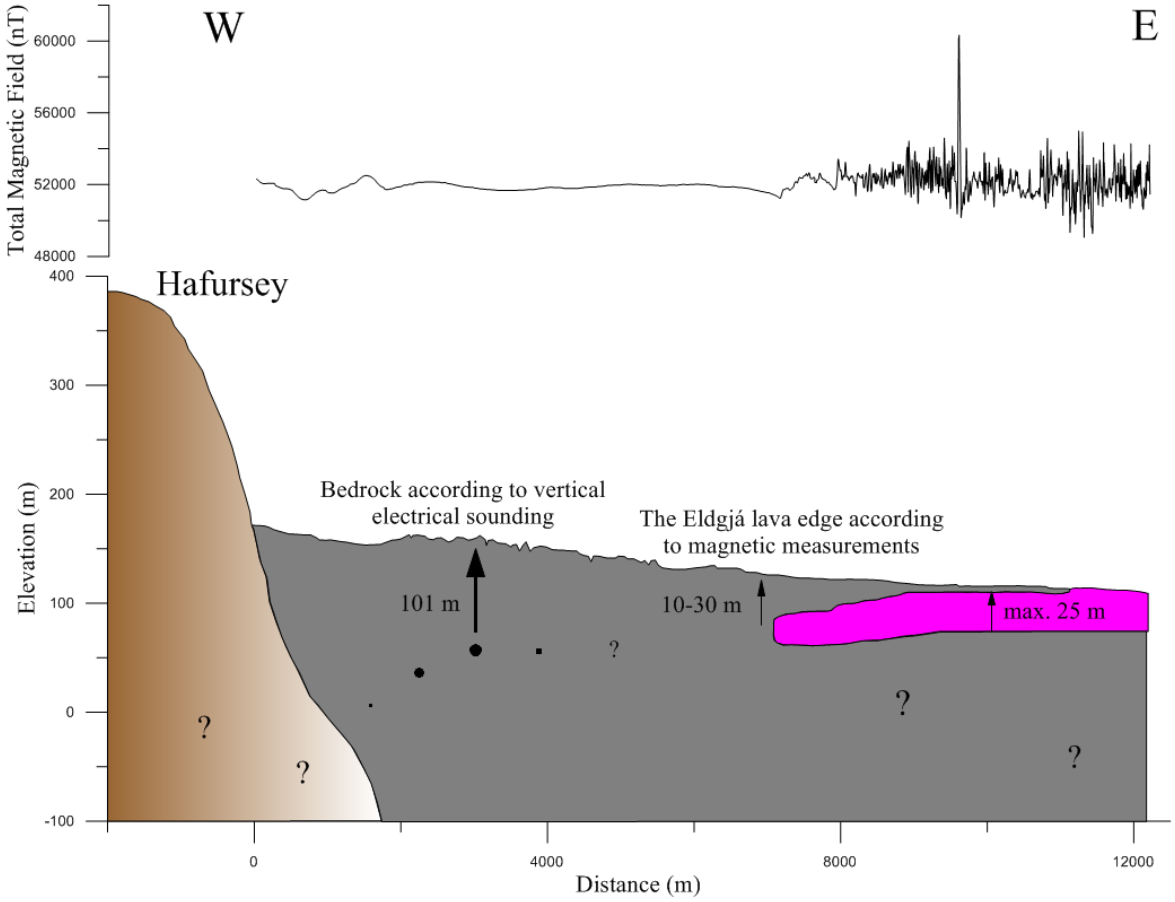

Figure 4.12: Cross section model of profile 4.

On profiles 6, 7, 9, 10 (Fig. 4.9) and 12 (Fig. 4.10) the lava flow lies at shallow depth under Mýrdalssandur. The depth decreases to the east and northeast towards the lava flow on the surface. However, the edge of the lava flow below the sand is not visible on the magnetic profiles and thus must lie west and southwest of the profiles (Fig. 4.11).

Profile 8 (Fig. 4.8) is the longest profile of the study or 15000 m and goes from the edge of Kötlujökull glacier southeast to the lava flow on the surface. The difference between the magnetic field above a deep source and a shallow source is seen but not as clearly as in profiles 4 and 5. Depth to magnetic sources on central Mýrdalssandur is comparable to depth to bedrock according to vertical electrical soundings (Thórarinsson and Guðmundsson, 1979). Here the depth is estimated to be 99 – 110 m and according to electrical soundings closest to the profile the bedrock is at maximum 122 m depth. The edge is located 8 km northeast of Hafursey at 10 – 27 m depth (Fig. 4.11). There the anomaly amplitudes increases as the anomaly spacing decreases. Peters half slope method therefore suggests a significant decrease in the depth to magnetic sources.

Profile 11 (Fig. 4.10) close to Rjúpnafell Mountain shows the lava flow beneath Mýrdalssandur and how it gets shallower to the northeast until it is being measured on the surface. The lava edge is located 8 km northeast of Hafursey at 5 – 10 m depth (Fig. 4.11). The edge of the lava lies much shallower here than on profiles 4 and 5 possibly due to less sediment accumulation or a thicker lava edge.

On profile 12 (Fig. 4.10) the magnetometer is measuring a shallow magnetic source most likely the Álftaver lava flow. However, the depth to magnetic rock alternates and gets deeper from section 1 to section 2 but then decreases until the lava flow is being measured on the surface in the northeastern most section. The lava edge could be located between sections 2 and 3 or southwest of the profile. Section one can also be reflecting other lava flows below Mýrdalssandur such as the Hólmsá lava flow.

Profiles 13 and 14 show different signatures than other profiles. Depth estimations indicate alternating between increasing and decreasing depths to the magnetic sources across the profiles. Possibilites are that here several different lava flows are being measured such as the Hólmsá- and Eldgjá lava flow and the Kriki hyaloclastite flow. The Kriki flow lies under Kötlujökull and extends 6-7 km from its margin where it disappears below sediments. The Kriki flow is a combination of subaerial and pillow lava, hyaloclastite breccia and hyaloclastite tuff, which all have different remanent magnetization (Table 3.1). The extent of the Kriki flow is not known and could thus be located below profiles 13 and 14. The contact between the Álftaver lava flow and the Kriki flow is not visible so the Álftaver lava flow could possibly lie below the Kriki flow (Larsen, 2000; 2010). Another influencial factor might be coming from the advance of the Kötlujökull glacier in 1600 BP (Schomacker et al., 2003). The glacier advanced some 3.5 – 5.5 km from its present position pushing sediments and affecting sediment thicknesses close to the glaciers snout leaving piles of sediments in some regions while excavating them in others. Thus, the sediment thickness above the Eldgjá lava flow on profiles 13 and 14 might vary. This is however only a minor contribution where several jökulhlaups have come down Mýrdalssandur since the advance of the glacier leaving sediments on top of the disturbances left behind by the glacier.

This study shows that magnetic measurements is a good tool for identifying buried lava flows (Nelson et al., 2014). The location of the buried lava edge can be identified to a good accuracy if measured correctly. The depth to the lava flow can also be estimated with good certainty with the Peters half slope method. However, to get a precise depth estimate more elaborate computed algorithms have to be used (Hinze et al., 2013).

4.4.2 Sedimentation rates at Mýrdalssandur

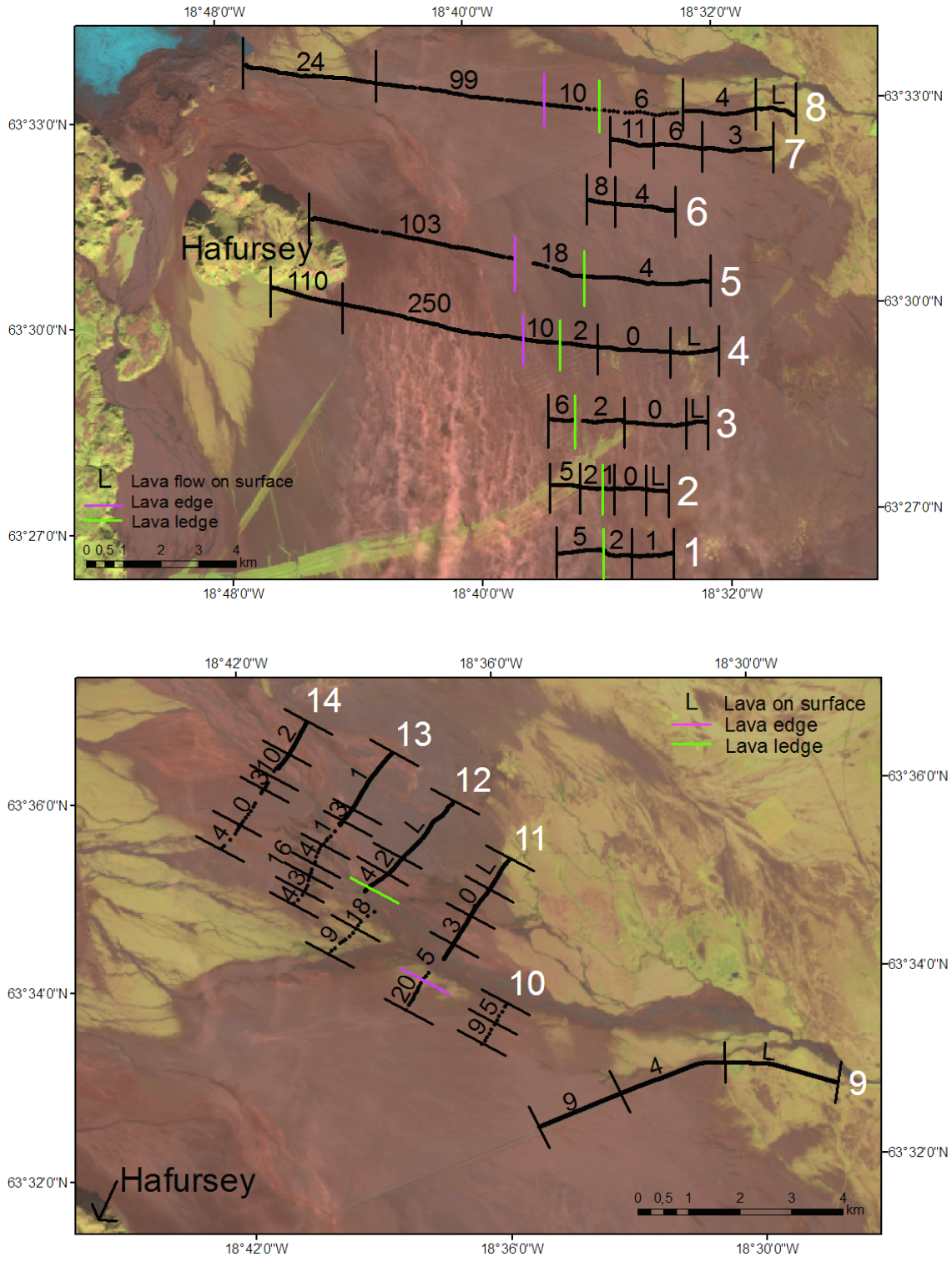

Figure 4.13: Maximum depth estimation map of Mýrdalssandur. Depth is given in meters for each section previously determined. Profiles are marked 1 – 14. Green lines are the locations of lava ledges and the purple lines are the locations of lava edges as determined previously in this study (Chapter 4.3.1) . Satellite image from United States Geological Survey (2014).

The depth to the assumed lava edge allows an estimate to be made of sedimentation rates at Mýrdalssandur since the Eldgjá lava flow was emplaced. Four profiles show evidence of a buried lava edge. Three of them suggest that the top of the lava flow at its edges is at ~10 m depth. Although, on profile 8 depth estimations indicate that the lava flow lies slightly deeper or at 18 m probable due to error in the magnetometer (Fig. 4.13). Figure 4.13 shows the thickness of the sediments on top of the Eldgjá lava flow, according to the Peters half slope method. The thickness of the lava flow according to borehole data is 18 – 25.0 m thick (Vegagerðin, 2013). However, lava flows are often thinner near the edges and this apparently applies to the Álftaver lava flow. This is supported by the existence of the buried lava ledges (Fig. 4.13). However, a possibility is that the porous upper part of the lava flow has been removed by jökulshlaups coming down Mýrdalssandur where dense basalt is seen on the surface in some parts of Mýrdalssandur (Vegagerðin, 2013).

Figure 4.14 illustrates the estimated thinning of the Eldgjá lava flow beneath Mýrdalssandur. The thickness of the sediments on top of the lava flow is estimated to be ~10 m. A rough estimate of the thickness of the sediments that have accumulated at Mýrdalssandur since the Eldgjá eruption in 934 is thus the thickness of the sediments on top of the lava flow (~10 m) and the thickness of the lava (~10 m) or ~20 m (Fig. 4.14). The area of the Mýrdalssandur west of the lava edge located in this study was calculated in ArcGIS and is 224 km^2.

$$224\ km^2 \times 0.020\ km = 4.50\ km^3$$

This value is of course very approximate and it may be more appropriate to use 4 – 5 km^3 as the post-Eldgjárlava accumulation. Even more sediments could have accumulated at Mýrdalssandur since the Eldgjá eruption because the Kerlingafjörður fjord was located west of Hjörleifshöfði, which has been filled and is not visible today. The southern coast also lay north of its current location, thus making it probable that the accumulation of sediments could be even more (Larsen, 2000).

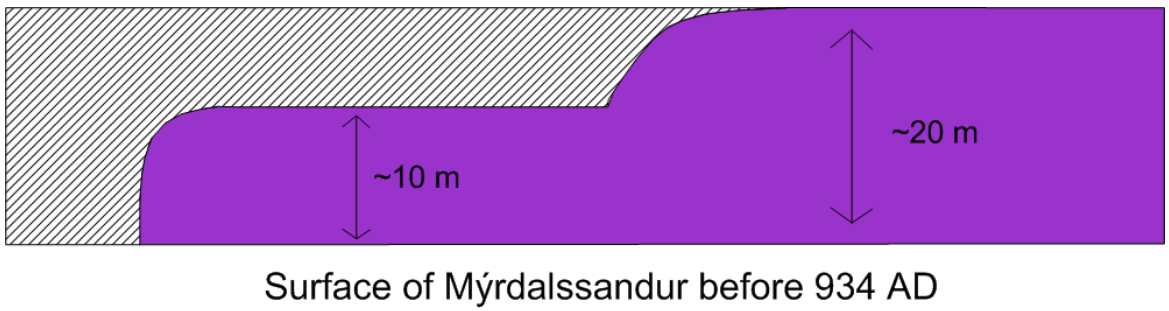

Figure 4.14: Thinning of The Eldgjá lava flow below Mýrdalssandur. The thickness of the lava flow decreases towards its edges from ~20 m to ~10 m. Thickness of sediments accumulated since the Eldgjá eruption is ~20 m.

The volume of sediments that accumulated on Mýrdalssandur in the jökulhlaup accompanying the 1918 Katla eruption, one of the biggest jökulhlaups, was 0.7 – 1.6 km^3 which covered an area of 700 km^2 (Tómasson, 1996; Larsen, 2010). Sediments also accumulated in the Álftaver area (0.05 km^3), at Kötlutangi (0.4 km^3) and 0.35 km^3 washed out to sea (Tómasson, 1996).

On profile 11 the thickness of the sediments on top of the lava flow is slightly less than in profiles at southern Mýrdalssandur or 5-10 m. Sedimentation at the northern Mýrdalssandur is possibly slower due to the higher flow rate of jökulhlaups closer to the glaciers snout so the particles do not settle as easily. It is also possible that the lava edge at northeast Mýrdalssandur is thicker than on other profiles as it is closer to the fissure. The lava flow would therefore have been a higher barrier and prevented the overflow of jökulhlaups for a longer time.

4.4.3 Area and volume of the Eldgjá lava flow

The Eldgjá eruption is one of the largest fissure eruption to occur in the last millennium covering an area of 780 km^2 (Larsen, 2000; 2010; Thordarson et al., 2001). However, it has not been possible to determine exactly the extent and thus the volume of the lava flow because of its partial burial beneath Mýrdalssandur sand plain. Estimates have ranged from 14 km^3 (Miller, 1989) to the newest estimates of 18.3 km^3 (Thordarson et al., 2001). The second largest basaltic lava flow in historic time is the Laki lava flow produced in the Laki eruption in 1783-1784. Its volume is 14.7 km^3 (Thordarson and Self, 2003). The volume of the Laki lava flow is better constrained than the Eldgjá's volume because it is one of the best documented basaltic fissure eruption and it is still not buried in sand anywhere. The Þjórsá lava flow of the Veiðivötn fissure system is the largest fissure lava eruption on Earth during the Holocene. The lava flow was produced in 8600 BP and is covered by younger lava flows but is estimated to be at ~25 km^3 (Hjartarson, 1988; Halldórsson et al., 2008).

Here it is assumed that the Eldgjá lava flow comprises the Álftaver-, Landbrot- and Meðalland lava flows combined (Larsen, 1979; 2000; 2010). It is known that the Álftaver lava flow was produced soon after the settlement of Iceland (Landnáma, 1968). The people living in the Álftaver area wrote about fires coming from the north. They had to evacuate to the west most likely due to lava flows advancing into the Meðalland and Landbrot areas. However, no written accounts are available from people in the Meðalland or Landbrot area. Álftaver was a highly populated area relative to Meðalland and Landbrot possibly because these areas were sand plains at the time of settlement and thus almost uninhabited. After the Eldgjá eruption the area would have been partly covered with new lava flows and sheltered from jökulhlaups. The existence of the new lava made these areas more favorable for people to live in. However, some debate has been about the age of the Landbrot lava flow and if it is of same age as the Álftaver lava flow (Larsen, 1979; Jónsson, 1987). Some believe that the Landbrot lava is of prehistoric age and is older than 5200 years and even older than 7000 years (Jónsson, 1987). However, most do agree that it is a part of the Eldgjá lava flow produced in 934 AD.

Here it is assumed that the Eldgjá lava flow is composed of all three branches, the Álftaver-, Meðalland- and Landbrot lava flows. The area of the lava flow below Mýrdalssandur estimated in this study is 64 km^2. When this value is added to the previous estimate of the area of the lava flow, the result is 844 km^2. Thus, the volume of the buried part estimated in this study 1.4 +/- 0.3 km^3 would have to be added to previous estimates of the lava flow of 18.3 km^3, resulting in ~19.7 km^3. This is 78% of the Þjórsá lava flow, the largest known fissure eruption in the Holocene. The volume could be even larger where the edge of the lava flow cannot be mapped out in the southern part of the study area (Profiles 1, 2 and 3). The edge could possibly lie even further to the west than has been estimated in this study (Fig. 4.11). The southern coast lied further to the north before the Eldgjá

eruption and the lava flowed partly into the ocean thus the southern study area could benefit from further observations. Although, not changing significantly the size, the results presented here underline what a major event the Eldgjá eruption was and highlighting that the Eldgjá lava flow is the second largest fissure eruption in the Holocene.

4.5 Conclusions

1. Abrupt decrease in depth to magnetic sources and significant increases in anomaly amplitudes are visible on the east side of roughly northwards trending boundary observed in several magnetic profiles on eastern Mýrdalssandur. These sudden changes are interpreted as resulting from the buried edge of the Eldgjá lava flow below Mýrdalssandur. The edge has been located on 4 profiles (4, 5, 8 and 11), being located 5 km east of Hafursey and 8 km south of Rjúpnafell (Fig. 4. 11).
2. Profiles 13 and 14 are not only measuring the Eldgjá lava flow. The profiles are located close to the Kriki hyaloclastite flow, which disappears below sand in the area of the profiles. The extent of the flow is not known and thus it might extend to the location of these profiles. Advances of the Kötlujökull glacier in 1600 BP could have affected the thickness of sediments closes to the glaciers snout, leaving piles of sediments in some regions while excavating them in others resulting in alternating thicknesses of sediments on top of the lava flow. However, because several jökulhlaups have come down Mýrdalssandur since the advance of the glacier this is a minor effect on the interpretations.
3. The depth to the top of the lava flow at the edges is at maximum 10 – 30 m. The depth is shallower in the upper part of Mýrdalssandur (profile 11) possibly due to a thicker lava edge than in many other localities or faster flow rate during jökulhlaups closer to the glacier. The overall interpretations of the profiles is that the estimated maximum depth to the top of the lava flow decreases towards the east and northeast, and becomes approximately zero on some profiles were the lava is visible at the surface.
4. The area and volume of the Eldgjá lava flow has been underestimated and with this study better estimates have been able to be done for further understanding of the event of the Eldgjá eruption.
5. The area of the lava flow buried below Mýrdalssandur, determined in this study, is 64 km^2 making the total area of the Eldgjá lava flow 844 km^2. The volume of the Eldgjá lava flow beneath Mýrdalssandur is estimated to be 1.4 +/- 0.3 km^3. The total volume of the Eldgjá lava flow is thus 19.7 km^3.
6. The sediment accumulation on central and western Mýrdalssandur since the Eldgjá lava flow was emplaced was estimated to be 4 – 5 km^3. It is most likely even more where the Kerlingafjörður fjord located west of Hjörleifshöfði has been filled with sediments since the Eldgjá eruption.
7. Further measurements are needed to determine the exact location of the lava edge east of Hjörleifshöfði but can be coarsly mapped (Fig. 4.11). The geology of the upper most profiles close to Kriki would also benefit from further measurements.

References

Bjarnason, I.Þ. 2008. An Iceland hotspot saga. *Jökull* 58: 3-16.

Björnsson, H., Pálsson, F. & Guðmundsson, M.T. 2000. Surface and bedrock topography of the Mýrdalsjökull ice cap, Iceland: The Katla caldera, eruption sites and routes of jökulhlaups. *Jökull* 49: 29-46.

Breiner, S. 1999. *Applications manual for portable magnetometers*. Geometrics, California, USA.

Einarsson, P. 1991. Earthquakes and present-day tectonism in Iceland. *Tectonophysics* 189: 261-279.

Einarsson, P. 2008. Plate boundaries, rifts and transforms in Iceland. *Jökull* 58: 35-58.

Elíasson, J., Larsen, G., Guðmundsson, M.T. & Sigmundsson, F. 2006. Probabilistic model for eruptions and associated flood events in the Katla caldera, Iceland. *Computational Geosciences* 10: 179-200.

Fei, J. & Zhou, J. 2006. The possible climatic impact in China of Iceland's Eldgjá eruption inferred from historical sources. *Climatic change* 76: 443-457.

Finaly, C.C., Maus, S., Beggan, C.D., Bondar, T.N., Chambodut, A., Chernova, T.A., Chulliat, A., Golovkov, V.P., Hamilton, B., Hamoudi, M., Holme, R., Hulot, G., Kuang, W., Langlais, B., Lesur, V., Lowes, F.J., Lühr, H., Macmillan, S., Mandea, M., Mclean, S., Manoj, C., Tangborn, A., Tøffner-Clausen, L., Thébault, E., Thomson, A.W.P., Wardinski, I., Wei, Z. & Zvereva, T.I. 2010. International geomagnetic reference field: the eleventh generation. *Geophys. J. Int* 183: 1216-1230.

Galeczka, I., Oelkers, E.H. & Gislason, S.R. 2014. The chemistry and element fluxes of the July 2011 Múlakvísl and Kaldakvísl glacial floods, Iceland. *Journal of Volcanology and geothermal research* 273: 41-57.

Geophysical Institute, University of Alaska Fairbanks. September 2014. *Aurora Forecast*. URL: www.gi.alaska.edu/AuroraForecast.

Georgsson, L.S. & Jóhannesson, H. 1979. *Segulmælingar við Skeggjastaði og Lambastaði í Hraungerðishreppi*. National energy authority, geothermal.

GEM systems. 2010. *GSM-19-T v7.0 Instruction manual*. Court Markham, ON Canada.

Grönvold, K., Óskarsson, N., Johnsen, S.J., Clausen, H.B., Hammer, C.U., Bond, G. & Bard, E. 1995. Ash layers from Iceland in the Greenland GRIP ice core correlated with oceanic and land sediments. *Earth and planetary science letters* 135: 149-155.

Gudmundsson, A. 2000. Dynamics of volcanic systems in Iceland: Example of tectonism and volcanism at juxtaposed hot spot and mid-ocean ridge systems. *Annu. Rev. Earth Planet. Sci.* 28: 107-140.

Guðmundsson, M.T. & Högnadóttir, Þ. 2006. *Ísbráðnun og upptakarennsli jökulhlaupa vegna eldgosa í Kötluöskju og austanverðum Mýrdalsjökli*. Report for the civil defence department of national commissioner. Reykjavík, Institute of Earth Sciences, 35 p.

Guðmundsson, M.T. & Larsen, G. 2013. Jökulhlaup. In: Júlíus Sólnes, Freysteinn Sigmundsson & Bjarni Bessason (editors): *Náttúruvá á Íslandi – Eldgos og jarðskjálftar*: 156-170. Viðlagatrygging Íslands/Háskólaútgáfan, Reykjavík.

Guðmundsson, M.T., Larsen, G., Höskuldsson, Á. & Gylfason, Á.G. 2008. Volcanic hazards in Iceland. *Jökull* 58: 251-268.

Guðmundsson, M.T. & Milsom, J. 1997. Gravity and magnetic studies of the subglacial Grímsvötn volcano, Iceland: Implications for crustal and thermal structure. *Journal of geophysical research* 102: 7691-7704.

Guðmundsson, O., Brandsdóttir, B., Menke, W. & Sigvaldason, G.E. 1994. The crustal magma chamber of the Katla volcano in south Iceland revealed by 2-D seismic undershooting. *Geophysical Journal Int.* 119: 277-296.

Hafliðason, H., Eiríksson, J. & Kreveld, S.V. 2000. The tephrochronology of Iceland and the North Atlantic region during the Middle and Late Quaternary: a review. *Journal of Quaternary Science* 15: 3-22.

Halldórsson, S.A., Óskarsson, N., Gronvold, K., Sigurdsson, G., Sverrisdóttir, S. & Steinthorsson, S. 2008. Isotopic heterogeneity of the Thjorsa lava – implications for mantle sources and crustal processes within the Eastern Rift Zone, Iceland. *Chemical geology* 255 (3-4): 305-316.

Hammer, C.U. 1984. Traces of Icelandic eruptions in the Greenland ice sheet. *Jökull* 34: 51-65.

Hinze, W.J., Frese, R.R.B.V. & Saad, A.H. 2013. *Gravity and magnetic exploration. Principles, practices and applications*. Cambridge University Press. Cambridge, The United Kingdom.

Hjartarsson, Á. 1988. Þjórsárhraunið mikla – stærsta nútímahraun jarðar. *Náttúrufræðingurinn* 58 (1): 1-16.

Jakobsdóttir, S.S. 2008. Seismicity in Iceland: 1994-2007. *Jökull* 58: 75-100.

Jakobsson, S.P. 1979. Petrology of Recent basalts of the Eastern Volcanic Zone, Iceland. *Acta Naturalia Islandica* 26: 109 pp.

Janowski, J. & Sucksdorff, C. 1996. *Guide for magnetic measurements and observatory practice*. International association of geomagnetism and aeronomy. Boulder, CO, USA.

Jóhannesson, H. & Sæmundsson, K. 1990. *Geological map of Iceland, sheet 6, South-Iceland, third edition*. Icelandic Museum of Natural History and Iceland Geodetic Survey, Reykjavík.

Jóhannesson, H. & Sæmundsson, K. 1998. *Geological map of Iceland. Bedrock geology, scale 1:500.000*. Náttúrufræðistofnun Íslands, Reykjavík (2nd edition).

Jónsson, G. & Kristjánsson, L. 2000. Aeromagnetic measurements over Mýrdalsjökull and vicinity. *Jökull* 49: 47-58.

Jónsson, J. 1982. Notes on the Katla volcanogenic debris flow. *Jökull* 32: 61-68.

Jónsson, J. 1987. Eldgjárgos og Landbrotshraun. *Náttúrufræðingurinn* 57 (1-2): 1-20.

Keary, P. & Brooks, M. 1984. *An introduction to geophysical exploration. Second edition.* Blackwell scientific publications, London, England.

Kristjánsson, L. 1985. Bergsegulmælingar – nytsöm tækni við jarðfræðikortlagningu. *Náttúrufræðingurinn* 54(3-4): 119-130.

Lacasse, C., Sigurdsson, H., Carey, S.N., Jóhannesson, H., Thomas, L.E. & Rogers, N.W. 2006. Bimodal volcanism at the Katla subglacial cladera, Iceland: insight into the geochemistry and petrogenesis of rhyolitic magmas. *Bull Volcanol DOI 10.1007/s00445-006-0082-5*.

Landnámabók, íslenskt fornrit I. Hið íslenska fornritafélag, Reykjavík 1968.

Larsen, G. 1979. Um aldur Eldgjárhrauna. *Náttúrufræðingurinn* 49: 1-26.

Larsen, G. 2000. Holocene eruptions within the Katla volcanic system, south Iceland: Characteristics and environmental impact. *Jökull* 49: 1-28.

Larsen, G. 2010. Katla: Tephrochronology and eruption history. *Developments in quaternary sciences* 13: 23-49.

Larsen, G. & Ásbjörnsson, S. 1995. Volume of the tephra and rock debris deposited by the 1918 jökulhlaups on western Mýrdalssandur, South Iceland. Abstract, *International Glaciological Society*, 20-25 August 1995, Reykjavík.

Larsen, G., Newton, A.J., Dugmore, A.J. & Vilmundardóttir, E.G. 2001. Geochemistry, dispersal, volumes and chronology of Holocene silicic tephra layers from the Katla volcanic system, Iceland. *Journal of Quaternary Science* 16(2): 119-132.

Lowrie, W. 2007. *Fundamentals of Geophysics. Second edition.* Cambridge University Press. Cambridge, The United Kingdom.

Maus, S., Macmillan, S., McLean, S., Hamilton, B., Thomson, A, Nair, M. & Rollins, C. 2010. *The US/UK world magnetic model for 2010-2015, NOAA Technical report NESDIS/NGDC*.

Miller, J. 1989. The 10th century eruption of Eldgjá, southern Iceland. *Nordic Volcanological Institute Report 8903*: 30pp.

Milsom, J. 2003. *Field geophysics. The geological field guide series. Third edition*. John Wiley & Sons, Ltd. West Sussex, England.

Mussett, A.E. & Khan, M.A. 2000. *Looking into the Earth.* Cambridge University Press. New York, USA.

Nelson, P.N., Whitehead, P.W. & Link, C.A. 2014. Buried lava flow crossing the Great Divide in north Queensland: discovery using magnetic methods, and implications for hydrology. *Australian journal of earth sciences: An international geoscience journal of the geological society of Australia* 57 (3): 279-289.

Norðdahl, H. & Hafliðason, H. 1992. The Skógar tephra, a Youner Dryas marker in North Iceland. *Boreas* 21: 23-41.

Nummedal, D., Hine, A.C. & Boothroyd, J.C. 1987. Holocene evolution of the south-central coast of Iceland. In: Fitzgerald, D.M., Rosen, P.S. (Eds.), *Glaciated coasts*. London. Academic Press: 115-150.

Óladóttir, B.A., Larsen, G., Þórðarson, Þ. & Sigmarsson, O. 2005. The Katla volcano S-Iceland: Holocene tephra stratigraphy and eruption frequency. *Jökull* 55: 53-74.

Óladóttir, B.A., Sigmarsson, O., Larsen, G. & Thordarson, T. 2008. Katla volcano, Iceland: magma composition, dynamics and eruption frequency as recorded by Holocene tephra layers. *Bull volcanology* 70: 475-493.

Peters, L.J. 1949. The direct approach to magnetic interpretation and its practical application. *Geophysics* 14 (3): 290-320.

Reynolds, J.M. 1997. *An Introduction to Applied and Environmental Geophysics.* John Wiley & Sons Ltd. West Sussex, England. 800 pp.

Russell, A.J., Tweed, F.S., Roberts, M.J., Harris, T.D., Guðmundsson, M.T., Knudsen, Ó. & Philip, M.M. 2010. An unusual jökulhlaup resulting from subglacial volcanism, Sólheimajökull, Iceland. *Quaternary science reviews* 29 (11-12): 1363-1381.

Schomacker, A., Krüger, J. & Larsen, G. 2003. An extensive late Holocene glacier advance of Kötlujökull, central south Iceland. *Quaternary science reviews* 22: 1427-1434.

Segulmælingastöðin í Leirvogi. September 2014. URL: http://www.raunvis.hi.is/~halo/leirvogur.html.

Sigmundsson, F. 2006. *Iceland Geodynamics. Crustal deformation and divergent plate tectonics series.* Praxis publishing, Springer Verlag, Chichester, UK, 209 pp.

Stothers, R.B. 1998. Far reach of the tenth century Eldgjá eruption, Iceland. *Climatic Change* 39: 715-726.

Sturkell, E., Einarsson, P., Roberts, M.J., Geirsson, H., Guðmundsson, M.T., Sigmundsson, F., Pinel, V., Guðmundsson, G.B., Ólafsson, H. & Stefánsson, R. 2008. Seismic and geodetic insight into magma accumulation at Katla subglacial volcano, Iceland: 1999 to 2005. *Journal of Geophysical Research* 113: B03212.

Sæmundsson, K. 1982. Calderas in the neovolcanic zones of Iceland. *Eldur í norðri*. Sögufélag Reykjavíkur: 221-239.

Telford, W.M., Geldart, L.P. & Sheriff, R.E. 1990. *Applied Geophysics*. *Second Edition.* Cambridge University Press. Cambridge, The United Kingdom.

Thorarinsson, S. 1955. Myndir úr jarðsögu Íslands III. Eldgjá. *Náttúrufræðingurinn* 25: 148-153.

Thorarinsson, S. 1957. The Jökulhlaup from the Katla area in 1955 compared with other jökulhlaups in Iceland. *Jökull* 7: 21-25.

Thorarinsson, S. 1975. Katla og annáll Kötlugos. *Árbók Ferðafélags Íslands 1975*: 125-149.

Thorarinsson, S. 1980. Langleiðir gjósku úr thremur Kötlugosum. *Jökull* 30: 65-73.

Thorarinsson, S. 1981. Greetings from Iceland. *Geografiska Annaler* 63A: 109-118.

Thordarson, T., Miller, D.J., Larsen, G., Self, S. & Sigurdsson, H. 2001. New estimates of sulfur degassing and atmospheric mass-loading by the 934 AD Eldgjá eruption, Iceland. *Journal of Volcanology and Geothermal Research* 108: 33-54.

Thordarson, T. & Self, S. 2003. Atmospheric and environmental effects of the 1783-1784 Laki eruption: A review and reassessment. *Journal of geophysical research* 108: 1-27.

Thordarson, T. & Larsen, G. 2007. Volcanism in Iceland in historical time: Volcano types, eruption styles and eruptive history. *Journal of Geodynamics* 43: 118-152.

Thordarson, T. & Höskuldsson, Á. 2008. Postglacial volcanism in Iceland. *Jökull* 58: 197-228.

Thórarinsson, F. & Guðmundsson, H. 1979. *Mýrdalssandur. A geophysical survey*. Natioanl energy authority.

Tómasson, H. 1996. The jökulhlaup from Katla in 1918. *Annals of Glaciology* 22: 249-254.

United States geological survey. June 2013. Earth explorer. URL: http://www.earthexplorer.usgs.gov.

Vegagerðin. 2013. *Grjótnám á Mýrdalssandi fyrir rofvarnir við Múlakvísl árið 2013*. Stapi Jarðfræðistofa.

Watsegård, S. 2002. Early to middle Holocene silicic tephra horizons from the Katla volcanic system, Iceland: new results from the Faroe Islands. *Journal of Quaternary Science* 17(8): 723-730.

Wastegård, S., Wohlfarth, B., Subetto, D.A. Sapelko, T.V. 2000. Extending the known distribution of the Younger Dryas Vedde Ash into northwestern Russia. *Journal of Quaternary Science* 15(6): 581-586.

Zielinski, G.A., Germani, M.S., Larsen, G., Baillie, M.G.L., Whitlow, S., Twicker, M.S. & Taylor, K. 1995. Evidence of the Eldgjá (Iceland) eruption in the GISP2 Greenland ice core: relationship to eruption processes and climatic conditions in the tenth century. *The Holocene* 5: 129-140.